Fifth Semiannual Progress Report
to
the National Aeronautics and Space Administration
on
the TM Project

"UTILIZING REMOTE SENSING OF THEMATIC MAPPER DATA TO IMPROVE OUR UNDERSTANDING OF ESTUARINE PROCESSES AND THEIR INFLUENCE ON THE PRODUCTIVITY OF ESTUARINE-DEPENDENT FISHERIES"

Joan A. Browder
Southeast Fisheries Center
National Marine Fisheries Service
75 Virginia Beach Drive
Miami, Florida 33149

L. Nelson May, Jr.
Coastal Fisheries Institute
Center for Wetland Resources
Louisiana State University
Baton Rouge, Louisiana 70803

Alan Rosenthal
Southeast Fisheries Center
National Marine Fisheries Service
75 Virginia Beach Drive
Miami, Florida 33149

Robert H. Baumann
Center for Energy Studies
Louisiana State University
Baton Rouge, Louisiana 70803

James G. Gosselink
Coastal Ecology Institute
Center for Wetland Resources
Louisiana State University
Baton Rouge, Louisiana 70803

June 10, 1988

INTRODUCTION

The continuing disintegration of the coastal marshes of Louisiana is one of the major environmental problems of the nation. The average rate of loss for the last 20 yrs has been approximately 104 sq km/yr (Gagliano et al 1981). At this rate, Louisiana's coastal marshes will all be gone in 145 yrs. Prevailing evidence suggests that the marsh disintegration results from local imbalances between building processes, such as sedimentation and the growth and accumulation of dead vegetative matter, and destructive processes, such as sea-level rise, crustal subsidence, erosion, and compaction (Gosselink 1984). Local elevation gradients within the marsh are so low that small changes in water level or land elevation can cause large changes in land and water area (Sasser 1977, Baumann 1980). Water management structures, navigation cuts and channels, and other alterations by man appear to accelerate the disintegration rate (Johnson and Gosselink 1982, Turner et al. 1982, Dozier 1983, Gosselink 1984).

The problem of marsh loss in Lousiana is relevant to fishery management because Louisiana leads the nation in landings of fishery products, and most of the landed species are dependent upon estuaries and their associated tidal marshes. Coastal marshes contribute to estuarine food chains through the export of organic detritus; and the shallow, protected waters of marshes serve as fish and shellfish nursery grounds, promoting survival and growth of the young.

Remote sensing studies by Faller (1979), Dow (1982), and Gosselink (1984) suggest that the abundance of fishery species is more strongly correlated with the length of the interface between land and water in the marsh (shoreline) than with actual area of marshland. Observations from a field study by Zimmerman et al (1984) support this conclusion. Simulations from a theoretical computer model by Browder et al (1984) suggested that land-water interface initially increases with marsh disintegration but reaches a maximum when the marsh is 50% water and decreases thereafter. The degree of change in interface with each incremental loss of marsh land and the maximum length of interface attained are a function of the order in which segments of land are converted to water and the resultant pattern of distribution of land and water. The more clustered the segments of land converted to water, the lower the rate of change and less the maximum interface.

In evaluating the potential effect of marshland loss on fisheries, the first two critical factors to consider are: (1) whether land-water interface in actual disintegrating marshes is currently increasing or decreasing, and (2) the magnitude of the change.

In the present study, Landsat Thematic Mapper (TM) data covering specific sample marshes in coastal Louisiana were used to (a) test conclusions from the Browder et al (1984) model with regard to the stage in disintegration at which maximum interface occurs; (b) to further explore the relationship between maximum interface and the pattern of distribution

of land and water suggested by the model; and (c) to determine the direction and degree of change in land-water interface in relation to land loss in actual marshes.

There are several reasons why Louisiana's coastal marshes were ideally suited for examination from this viewpoint. First, large contiguous expanses of marsh are present, enabling us to obtain large sample areas containing only wetland. Second, many scientific investigations concerning ecological principles, geologic processes, and experimental use of remote sensing techniques have been made in this region. Third, geologic changes are occurring very rapidly here, and fourth, Louisiana's coastal marshes are the most extensive in the United States and support a high proportion of total U. S. production of estuarine-dependent fish and shellfish.

The coastal wetlands of Louisiana were formed as deltas of the Mississippi River and its tributaries. The large, heterogeneous expanse of deltaic wetlands along the Louisiana coast is extremely young geologically. It was formed within the past 3,000-5,000 yrs B.P. via a series of overlapping deltaic lobes of differing ages (Fig. 1). Instability is a characteristic of youthful geologic environments. Subsidence, a complex set of processes, has pronounced effects on near sea-level wetlands. Isostatic adjustments in the form of crustal downwarping from sedimentary loading, tectonic processes that occur contemporaneously such as folding, fracturing, flowing, and growth faulting, consolidation of underlying sediments due to the weight of natural features (e. g., natural levees), and differential compaction related to textural variability are among those natural processes involved in submerging this coastline. Human activities in the form of fluid withdrawals (hydrocarbons and water), marsh dewatering through reclamation processes, and sediment consolidation resulting from building structures in wetlands, all exacerbate coastal submergence. The above subsidence factors, combined with eustatic sea level rise, have given coastal Louisiana the fastest submerging coastline in the United States (Hicks 1981).

Submergence results in the "drowning" of marshes and their conversion to bay and lake environments. Combating the effects of submergence is sedimentation via the Mississippi River and its tributaries, which is responsible for Mississippi delta lobe development. The geologic record indicates that, on the average, a major delta lobe complex will develop and enlarge over a period ca. 1,000 yrs. This is followed by an abandonment period characterized by wetland loss, also of ca. 1,000 yrs. During this abandonment period, however, another delta lobe complex is simultaneously developing. Throughout at least the Holocene, the Mississippi Deltaic Plain has always concurrently exhibited areas of development and abandonment. Presently, however, the leveeing of the Mississippi River and maintenance of its present course, combined with reductions in sediment loads (Tuttle and Combe 1981) and debouchment of sediment at the edge of the continental shelf, have resulted in widespread wetland loss. The construction of ship channels, pipeline canals, and access canals for hydrocarbon exploration and production has both contributed to and accelerated these losses. Acceleration occurs through the effect of these structures on salinity distributions and sediment deposition. For instance, canals pro-

mote salt water intrusion, which results in the death of brackish-water marsh vegetation, retarding the accumulation of organic soils. Spoil banks associated with canals prevent sediment from being deposited on the marsh surface and reduce exchanges of water and materials between the marsh and open water. The natural geologic process of wetland deterioration, which would otherwise take place over several centuries, appears to now have been compressed into several decades.

Four major types of Louisiana coastal marshes have been distinguished by Chabreck (1972) on the basis of vegetation: fresh, intermediate, brackish, and saline. Several investigators have found significant differences among these marsh types in various soil, water quality, and other parameters, thereby supporting Chabreck's separation. Gosselink et al. (1979) found considerable differences in the length of land-water interface per-unit-area among the four marsh types in the neighboring Chenier Plain (Marginal Mississippi Deltaic Plain) of southeast Texas and southwest Louisiana.

Sasser et al (1986) used photointerpretation of aerial photographs, in combination with a computer-based geographic information system (GIS), to detect change in the percent water within wetlands on the Late Lafourche delta lobe. They found a pattern of general degradation in wetland area: marshes were degrading into various densities of shallow water bodies. In 1945, 91% of the marsh and natural levee area was solid or less than 10% water. By 1956, only 77% of the marsh was less than 10% water, by 1969 only 46%, and by 1980 only 28%. They noted two patterns of disintegration: (1) small, randomly-spaced water bodies developing within solid marshes and gradually growing into larger water bodies and (2) loss of land along the margins of major water masses, as if by mechanical wave attack, or erosion. The first effect seemed to be the more important.

A study in Chesapeake Bay by Rosen (1977) indicated that shorelines with low tidal ranges have higher rates of erosion than areas with higher tidal ranges, possibly because higher tidal ranges form higher elevation beaches; storm sturges are less likely to reach the elevation of fastland (bluff of dune) material to augument erosion, and wave energy is distributed over a greater distance in the course of a tidal cycle. The tidal range in Chesapeake Bay varies from 0.36 m to 1 m over a distance of 120 km. The tidal range in the north-central Gulf of Mexico is approximately 0.6 m.

Liebowitz and Hill (in press) used digital habitat maps for 1956 and 1978 from the U.S. Fish and Wildlife Service (Wicker 1980) to quantify change in coastal marshes during the 22-yr period and to evaluate various possible causes of the change. Their study covered the two areas covered by the present study - the late Lafourche lobe and the early Lafourche lobe (referred to as Terrebonne in their study). Water, wetland, and upland could be distinguished in the data, which had been classified according to the Cowardin et al (1979) system. Boundaries between saline and freshwater zones were also defined, based on vegetation. Liebowitz and Hill (in press) classified each map cell on the basis of a comparison of 1956 and 1978 habitat maps, as follows: areas that were fresh in 1956 and fresh in

1978; areas that were fresh in 1956, but saline in 1978; areas that changed from saline to fresh between 1956 and 1978; and areas that remained saline during the 22-yr period. They also identified the cells in each habitat category that changed from land to water during the 22-yr period. Their results indicated a 37% net area change from salt to fresh on the late Lafourche lobe and a 16% net area change from fresh to salt on the early Lafourche lobe. The highest rate of land loss on the late Lafourche lobe was 27% and occurred in the fresh-to-salt area. The highest rate of land loss on the early Lafourche lobe was 16% and occurred in the fresh-to-fresh area. By statistical comparisons, they ruled out salt-water intrusion as a reason for land loss on the early Lafourche lobe but concluded that it could be a cause of land loss on the late Lafourche lobe. The highest loss rates - 47 to 55% - occurred in the mudflat and beach/dune/reef habitats. Loss rates in fresh and saline marsh averaged approximately 18%. Loss from shoreline erosion accounted for only 2.1% (early Lafourche) and 3.2% (late Lafourche) of all land loss. Thus, the major form of land loss for all three regions was the conversion of land to inland open water (lakes, ponds, or bays).

Several studies have utilized simulated thematic mapper (TMS) and Landsat MSS imagery with collateral data, such as fish abundance and vegetative biomass, to examine the role of coastal wetlands in estuarine food chains and the production of estuarine-dependent fish and shellfish. These studies were supported by the development of software routines used to determine shoreline density (Faller 1977) and shoreline length (Faller 1977, Dow and Pearson 1982), to identify water bodies (Butera 1982a), and to measure the distance between land-cover classes (Butera 1982b). Faller (1979) found a good correlation between shrimp yields and shoreline density in subareas of the Louisiana coastal zone. Dow (1982) expanded Faller's (1979) approach and developed predictive equations that related the abundances of selected species of fish and shellfish to shoreline-length estimates for subareas of Apalachicola Bay, Florida. The findings of both authors suggest that abundances of some fish and shellfish could be influenced by the density and length of the marshland-water interface. Butera and Seyfarth (1981) and Butera et al. (1984) used water-body identification, distance measures, shoreline density, and vegetative biomass estimates to quantify organic carbon export into nearby water bodies.

The model used in this study is the second generation of a stochastic spatial computer model introduced by Browder et al (1984). In the initialization of the model, marsh dimensions are defined in terms of the numbers of rows and columns of pixels. Each pixel can exist in one of two states, land (emergent vegetation) or water. Initially, all the pixels are land and the marsh is solid. One land pixel is converted to water at each iteration. The actual pixel converted is determined by a random number generator linked to a probability function that incorporates two weighting factors. The weighting factor values assigned to each pixel determine its relative probability of disintegrating at each iteration. The first, W, determines disintegration probability on the basis of the number of sides that the pixel is bordered by water. The second, G, governs the probability that the pixel will disintegrate if it borders the main water body. The probability weight of each pixel is calculated by the equation:

$$F_{i,j,k} = 1 + W\,S_{i,j,k} + G_1\,B1i,j + G_2\,B12i,j + G_3\,B3i,j + G_4\,B4i,j \quad (1)$$

where W = weight coefficient for each side adjacent to water, S = number of sides adjacent to water, G = weight coefficient for pixels adjacent to a major outside water body, and B = a Boolean value (1 or 0) indicating whether the pixel is adjacent to a major outside water body. The probability weight of a given pixel changes throughout the simulation, depending on what happens to other pixels, particularly those adjacent to it.

The weighted probability function approximates the natural processes of eating away from the center (the W factor) and erosion due to tidal action or wind/induced turbulence along the edge of major water bodies. In taking this approach, we did not assume that marsh loss is a random process but merely that the process coud be simulated by a weighted randomly-driven function.

The model simulates the entire process of disintegration, starting with solid land and ending with solid water. Each iteration represents the passage of time, although the units of time are not specified.

At each iteration of the simulation, a counter keeps track of the percent area as water, referred to throughout this discussion as the "level of disintegration", and the length of the land-water interface. The latter is expressed in terms of pixel-lengths, the length of one side of the square pixel; therefore, measuring interface length consisted of counting the number of "joins" between land pixels and water pixels. Thus, interface, as we measured it, is exactly homologous to the "black-white join" (J), the spatial autocorrelation parameter introduced by Moran (1948) into the literature of quantitative geography. Upton and Fingleton (1986) described the common relationship between the join statistic and other spatial pattern paramaters such as that of Cliff and Ord (1973) and defined the cross-product statistic, R, which is equal to 2 x J.

Upton and Fingleton (1986) provide an intricate set of equations for calculating R, the expected value of R [E(R)], and the variance of the expected value. E(R) assumes a random distribution of black and white (or land and water) cells. R departs from E(R) to the extent that like-cells are clumped [R < E(R)] or uniformly distributed [R > E(R)]. They provide simpler equations for calculating J, E(J), and var E(J) for cases in which the area is regular-sided and square in configuration (their equations for the R statistics are more general). In our simulations, we were able to determine J simply by keeping a running total of the number of land-water joins created at each conversion of a land pixel to a water pixel. A method related to counting was used to determine the number of land-water joins in land-water classified satellite imagery. Our observations suggest that, for a square area with regular sides, E(J) is approximately equal to one half the number of land-water joins of an area of the same dimensions having a checkerboard pattern of distribution of land and water. This can be calculated as follows:

$$E(J) = 2\,N^2 - 4\,N \quad (2)$$

where N = the number of rows = the number of columns

The weighting factors affect the order of disintegration of marsh land pixels and the resultant distribution of land and water in the simulated marsh. The higher the values of the weighting factors, the more clumped the water pixels. By affecting the spatial distribution of water pixels, the weighting factors determine interface length in simulated marshes. Taking advantage of this relationship, the approach we took to simulating the disintegration of actual marshes was to use spatial pattern, as expressed by level of disintegration, interface length, and other spatial pattern statistics of the actual marshes, compared to those from simulated marshes, to select W and G weighting factors for the model. The other spatial pattern statistics that were used were: numbers of water pixels with zero, one, two, three, and four sides adjacent to other water pixels and numbers of water pixels on each of the marsh's four borders. The distribution of water pixels by size of water clusters at the current (i.e. December, 1984) level of disintegration was used to test the fit of the simulated marsh to the actual marsh. Comparison of simulated marshes to actual marshes in general suggests that the function will work well for simulating reticulated marshes such as those on the Gulf coast, although it might not work well for marshes with a more dendritic pattern of land and water, such as those found along the U.S. Atlantic coast.

METHODS

We expanded the model so that it could simulate marshes of substantial size, used actual marshes to calibrate the weighting factors of the model, and then used the model to simulate the disintegration over time of each sample marsh. Model calibration was accomplished by quantifying the spatial pattern statistics of the sample marshes and matching them to the spatial pattern statistics expected from simulated marshes, based on a series of simulations in which W, G, and the number of water borders (BC) were varied.

The study can be thought of as a process consisting of nine steps: (1) expansion, refinement, and sensitivity testing of the model; (2) selection of sample sites; (3) analysis of imagery; (4) measurement of spatial pattern parameters; (5) development of a knowledge base and an expert system; (6) calibration of the model to the sample marshes; (7) simulation of the disintegration patterns of the sample marshes; (8) evaluation of simulation results; and (9) interpretation.

Model Expansion, Refinement, and Sensitivity Testing

The first phase in the study was improving the model. Our improvements were guided by a series of sensitivity tests: (1) tests of the effects of the W and G weighting factors, varied separately, (2) tests of the

effect of marsh geometry (i.e. length, relative to width), and (3) tests of the effect of marsh size, in terms of number of pixels.

In the original version of the model, only the pixels initially on the major outside water body had the G weighting (B = 1). The G effect was inconsequential in sensitivity tests with the original model, particularly as the size of the marsh simulated was increased. Based on this observation, the model was revised so that any pixel, regardless of original location, could eventually be assigned B = 1. The G factor in the present version of the model has a much greater effect than that in the earlier version.

Other sensitivity tests indicated that the geometry of the marsh (i.e., ratio of length to width, affected the trajectory of change in interface relative to W and G and greatly complicated the process of examining interface as a function of W and G and the number of water borders to the marsh (i.e., simulation results differed depending upon whether a water border was the long or the short border). We decided to work with square marshes, both simulated and actual, in order to avoid this complication.

To eliminate another complicating variable - scaling - we decided to simulate marshes of the same size (same number of pixels) as our sample sites. We determined that it would be practical to simulate marshes up to 192 x 192 pixels, although not with replication. A 192 x 192 pixel site roughly covers 33.18 square kilometers and is approximately one quarter of the area covered by a 7.5-minute U. S. Geological Survey topographic map.

Increasing the size of the simulated marsh necessitated streamlining the algorithm for weighting disintegration probability and converting land pixels to water pixels. In the original algorithm, each pixel, identified by its x,y coordinate was repeated on the list the same number of times as its probability factor (F in equation 1). Each item on the list had a unique number, and the pixel selected was the one that corresponded to the random number at that iteration, providing it had not already been converted to water at a previous iteration. All occurrences of pixels that had been newly converted to water were cleared from the list at periodic intervals throughout the simulation. The process got slower and slower as the need for purging the list approached. This algorithm was too slow and awkward to be scaled up in the same form. In our revision, each pixel appears on the numbered list only once, but its probability factor is listed with it. Two random numbers are associated with each selection. The first random number makes a tentative selection and the second determines whether the pixel is eligible. Eligibility depends on whether the pixel's probability factor is larger than the random number. The selection process continues, with two new random numbers generated each time, until the selection of an eligible pixel is made. Of course, the first random number - the one that makes the tentative selection - is a uniform random number from 0 to 1 that is multiplied by the number of pixels on the list, and the second random number is a uniform random number from zero to 1 that is multiplied by the largest probability factor on the list. A pointer system keeps track of the pixels on the list and eliminates from the list

the pixel that has been converted to water at each iteration. A flow diagram of the new algorithm is presented in Figure 2.

The model and all ancellary programs were written in C and were executed on an AT&T PC-7300, a 16-bit computer that has a Unix-V operating system.

Study Site Selection

The study sites are located in salt and brackish marsh areas on two abandoned delta lobes of the Mississippi River, the early Lafourche and the late Lafourche. The early Lafourche lobe was an actively prograding lobe within the last 1,800 years; the late Lafourche lobe was active as a main distributary of the river within the last 600 years. On each lobe we selected sites that corresponded to the boundaries of five contiguous U.S. Geological Survey 7.5-min topographic maps (Fig 3). Areas defined by each topographic map were divided into four contiguous quarters, each encompassing an area 192 elements wide and 192 scan lines long on the TM image. The intersection of the four quarters was aligned to correspond to the center point of each topographic map. Each area corresponding to a quarter area of the ten topographic maps was a potential sample site. After excluding sites with upland vegetation and sites for which cloud-free TM imagery was not available, we had 72 samples to use in the study: 40 salt-marsh sites (20 on each lobe) and 32 brackish marsh sites (19 on the early Lafourche lobe and 13 on the late Lafourche lobe). Salt and brackish marshes were distinguished by means of the U.S. Fish and Wildlife Service habitat maps (Cowardin et al 1979).

Because of small errors in TM imagery, pixels are neither exactly square nor exactly the same size; therefore, it was necessary to eliminate several pixels on the outer boundaries of imagery corresponding to each topographic map in order to have a 192 x 192 image; therefore, our sample images do not provide complete coverage of the area - small strips at the boundaries of the topographic maps are missing. Selecting square samples - samples having the same number of rows and columns of pixels - greatly simplified the analyses of this study in several ways. First, we had fewer alternatives to consider in sensitivity analysis and constructing look up tables. Secondly, we could use simpler and less time-consuming equations for estimating spatial autocorrelation statistics. The quarter was the largest square unit into which a topographic map could be evenly divided that could be simulated with practicality in the same dimensions (192 x 192 pixels) by our computer model on available dedicated hardware.

Image Processing and Analysis

TM scenes were analyzed on the Fisheries Image Processing System (FIPS) maintained by NMFS in Slidell, Louisiana. FIPS uses a Sperry-Univac V77/600 mini-computer, color image display device, and other

hardware to process remotely sensed digital imagery. The software is a modified version of the Earth Resources Laboratory Applications Software (ELAS) (Graham et al. 1984).

The TM image acquired for the project represented one of the few relatively cloud-free images covering southern Louisiana (quads 1 and 2 in path 22 and row 40 of the World-Wide Reference System). The Landsat overflight occurred on 2 December 1984 (Scene ID: 50276-16022) and covers most of the Mississippi deltaic plain.

TM images of the sites were georeferenced to fit a Universal Transverse Mercator projection with a north-south orientation. The ELAS modules PMGC and PMGE (Graham et al. 1984) were used to accumulate ground control points, generate polynomial least-squares mapping equations, and resample the image using the bilinear interpolation technique. The average registration accuracies ranged from 22 to 56 m.

Land and water were distinguished in the TM images by first generating a product image from bands 4 and 5 and then applying the global thresholding technique developed by Pun (1981).

Measurement of Spatial Pattern Statistics

Seventy-two binary land-water images were generated from the product images of the salt and brackish marsh sites. Sequential ELAS commands set up for batch processing were used to measure the following spatial pattern parameters in each image: (1) total numbers of land and water pixels; (2) total numbers of water pixels by scan line and by element column; (3) the length of the land water interface, expressed as the total number of land-water joins; (4) total number of water pixels with sides adjacent to zero, one, two, three, and four other water pixels; and (5) water-body size frequencies. In determining the total number of water pixels with sides adjacent to other water pixels, the pixels at the boundary of the sample were excluded to avoid biasing the distribution of pixels toward those having less than four sides adjacent to water.

The total number of land-water joins in each image was tabulated using a three-step process. First, an intermediate image was generated using the ELAS shoreline-length (SLIN) module (Graham et al 1984). SLIN uses a 3 x 3 moving window technique to classify each land pixel adjacent to water into one of 69 shoreline categories (Dow 1982; Dow and Pearson 1982). Second, a look-up table (Appendix Table 1) was used to convert the SLIN image into an image file comprised of six classes: (1) land; (2) water; and (3) shoreline pixels with one, two, three or four sides adjacent to water. Finally, the total number of land-water joins in each sample site was determined by enumerating the number of land pixel sides bordering water pixel sides.

The total number of water pixel sides adjacent to other water pixels was tabulated using a modification of the technique used to count land-water joins. Two changes in the processing sequence were required: (1)

water pixels adjacent to land were defined as shoreline pixels during processing with the SLIN module and (2) an additional processing step with a new look-up table was required to correctly classify water pixels with zero, one, two, three, or four sides adjacent to other water pixels.

As Hutchinson (1957) originally pointed out and first Richardson (1961) and then Mandelbrot (1967) elaborated upon, the length of an irregular shoreline is, to some extent, a function of measurement unit. Our measurements of land-water joins and, possibly, the other spatial pattern statistics, are valid only at the resolution of the TM imagery, the 30 x 30-m pixel. Future measurements cannot be compared to ours unless the same measurement unit is used.

Selecting Probability Factors

Marsh study sites were classified according to whether they had one, two, three, or four water borders. Then a series of simulations run for each border combination were used to build a knowledge base to indicate how our spatial pattern statistics changed with variation in the two weighting factors, W and G. An expert system was developed to use this knowledge base to estimate the W's and G's to best approximate the land-water patterns of the sample marshes. By using the probability factors that best approximated the spatial patterns of the study sites, we then simulated the pathway of change in interface with disintegration for each site.

Classification of marshes according to water borders was accomplished by comparing the proportion of water pixels on each border to the proportion of water pixels in the marsh as a whole. Those borders having a higher proportion of water pixels than the entire site were assumed to be bordered by water. Classifications were confirmed by visual examination of black and white photographs of binary land-water images of the sites. In a few cases, classifications were changed based on the visual examination.

To build a knowledge base for use by the expert system, simulations were run with all possible W and G combinations from the set [0, 4, 20, 60, 180, and 540] for six types of study site border conditions: 0 = no water border, 1 = 1 water border, 2 = 2 adjacent water borders, 3 = 2 opposite water borders, 4 = 3 water borders, and 5 = 4 water borders. For border condition 0, the set was extended to include W = 1620 and 9720. Each simulation contributed information to 21 tables. Each table contained interface and side-adjacency (Adj-0, Adj-1, Adj-2, Adj-3, Adj-4) information collected at a 0.05 increment of disintegration level. Twenty-one tables (one for each increment of level) were compiled for each value of G and for each border condition (a total of 6 x 5 = 30 sets of 21 tables). For border condition 0 (no water border), there was only one set of 21 tables, since G must equal zero. For each of the other data sets, there were 21 tables for each G value.

The following statistics from each study site were used in the decision process: level of disintegration (D), interface (I) (same as the number of land-water joins), and number of water pixels having 0, 1, 2, 3,

and 4 sides adjacent to water, respectively (these are Adj-0, Adj-1, Adj-2, Adj-3, and Adj-4). Border condition (BC), having been estimated in the manner described above, was an additional factor in the decision process.

The level of disintegration was used to determine which tables were accessed. The tables of the nearest levels on either side of the study-site level were accessed. For instance, if the level of disintegration of the sample was 0.32 (32% water), then the tables for levels 0.30 and 0.35 were accessed. Interpolation between levels was then used to produce, for every G value and border condition, a table of values of spatial-pattern statistics for each of the six values of W for the specific level of disintegration of the study site.

Then, for each G value and border condition, the study-site interface and side-adjacency values were compared with values for these spatial pattern statistics in the tables prepared for the specific disintegration level. If the study-site value for a spatial pattern statistic was within the range of values for that statistic on a particular table, exact matching or interpolation between values was used to estimate W on the basis of that statistic, given the G value and border condition of that table. If the value of a given statistic from the study site was not within the range of values for that statistic in a table, it was not possible to obtain an estimate of W from that particular statistic and table.

Usually, several estimates of W were obtained for a given table. A weighted mean W for the specific G-value and border condition was obtained from these. In cases where a parabolic relationship between the parameter and W occurred, more than one estimate of W was sometimes obtained for the same statistic and table. In such cases, each estimate was used alternatively in calculating a weighted mean until all possible weighted means involving each spatial pattern statistic no more than once were calculated. For instance, interface might yield W = 2, 4; Adj-0, W = 180, 193; and Adj-3, W = 300. Then 2 x 2 x 1 weighted mean W's were calculated. One would involve 2, 180, and 300; another 2, 193, 300; another 4, 180, 300; and another 4, 193, 300. Weighting was a function of the number of water pixels involved in each parameter estimate of W. The value of the parameter was the estimate of the number of pixels involved in the estimate of W from that spatial pattern statistic.

parameter.

Weighted mean W's were calculated as follows:

$$\text{Weighted Mean } W = \text{Sum of } (W_i V_i) \;/\; \text{Sum of } (V_i) \qquad (3)$$

where W_i = the estimate of W from statistic i

V_i = the number of pixels involved (statistic value), statistic i.

Only the water pixels of the spatial pattern spatistics involved in the specific calculation of W were summed. As mentioned above, if the statistic value from the sample was not within the range of values for that statistic in a particular table, an estimate of W based on that statistic could not be obtained.

The coefficient of variation of each weighted mean W also was calculated. Coefficient of variation was calculated as follows:

$$\text{Coefficient of Variation of Mean W} = (\text{Variance})^{-1/2} / \text{Mean W.} \qquad (4)$$

In addition, the sum of the water pixels used in calculating the weighted mean W was retained as a "decision number" for later use in the selection process.

By the above process, many W-G-BC combinations were estimated for each study site. Weighted mean W's, coefficients of variation, and decision numbers and their corresponding G's and border-condition codes were stored in solution files specific to each study site. The file was sorted in descending order of decision number and, within decision number, in descending order of coefficient of variation of the weighted mean W.

The best solution was selected in the following manner:

Row and column data from the study-site imagery were used to classify borders. If the percent water pixels in the border row or column was greater than the percent level of disintegration of the study site, then that border was classified as water. Otherwise, it was classified as land. Examination of black and white photographs of binary land-water images of the study sites displayed on the CRT confirmed the appropriateness of this simple approach. In a few cases of obvious failure of the approach to reflect border conditions, classifications based on visual estimation were substituted. Visual inspection confirmed the automatic classification in all but a few study sites. Based on the border classification, each study site was assigned to a border-condition category.

Once the border condition of the study site was defined, the solution file specific to the spatial pattern statistics of that study site was searched for the "best" weighted mean W, specific to calculated G, for that border condition. If a solution having the right border condition was found in the group of solutions with the highest decision number (sum of the water pixels used in calculating the weighted mean W), it was selected as the best solution. If there was more than one solution having the right border condition in the group of solutions with the highest decision number, then the one with the lowest coefficient of variation was selected. If a solution having the right border condition could not be found within the group having the highest decision number, then we sought a solution with the right border condition among all solutions having decision numbers within 75% of the highest decision number. The solution having the right border condition, the largest decision number, and the lowest coefficient of variation was selected. If a solution having the right border condition was not found in either of the above groups, then solutions having alternative border conditions were considered. First, solutions with border conditions having no more than one border different from the right border condition were considered. Then, solutions with border conditions having no more than two borders different from the right border condition were considered. Usually, a solution was found having the right border condition or no more than one border different from that of the border condition initially defined.

RESULTS

Using the new model to simulate 48 x 48 pixel marshes, we explored (1) trajectories of disintegration under different settings of W and G and (2) variation in spatial pattern statistics with different settings of W and G. Working with simulated marshes having one water border, we learned that W and G have a highly nonlinear interactive effect on interface and other spatial pattern statistics. A plot of interface versus G under alternative settings of W is shown in Figure 4. Note that W exerts little effect at high settings of G, and G has little effect at high settings of W. As indicated in a graph showing trajectories of change in interface with disintegration from simulations under several settings of W and G and one water border (Figure 5), the trajectory of disintegration is symmetrical around 50% at all settings of W when G is zero or low. When G is high and W low, however, the trajectory is asymmetrical, with maximum interface occurring slightly to the right of 50%. The interaction of W and G apparently can affect the point of maximum interface in model simulations. This was not observed in simulations with the original model, in which G had virtually no effect.

Figures 6 through 10 show the interactive effect of W and G on the other spatial pattern statistics. Correlation tests with the 48 x 48-pixel simulations indicated that 'I' and Adj-4 were highly correlated, Adj-2 and Adj-3 were somewhat correlated with each other, and Adj-1 and Adj-0 were independent of each other and the other statistics.

The manner in which interface length (I=J) varies with W, G, and water-border condition (BC) in 192 x 192-pixel marshes is indicated in Table 1. These values were recorded at the 0.5 level of disintegration of the simulated marsh. Information on interface and the side-adjacency statistics were recorded throughout each simulation at each 0.05 interval of disintegration. These simulations were run to develop the look-up tables for the knowledge base used by the expert system. Several general aspects of the pattern of this data are apparent. Note that 'I' declines as the number of water borders increases. A complication relative to this relationship is that the two-adjacent-sides condition departs considerably from the two-opposite-sides condition when G is high, particularly when G is high relative to W. The nonlinear and highly interactive effect of W and G is another important aspect of the pattern of these data. At low G values, 'I' decreases with increases in W, whereas, when G values are high relative to W, 'I' increases with increases in W. This effect is most pronounced as the number of water borders increases. In Appendix Table 2, the W-G-BC combinations in Table 1 are listed in descending order of interface.

Table 2 shows the level of disintegration and measured spatial pattern statistics for 72 sample marshes (Louisiana study sites), according to thematic mapper imagery. The marshes are organized on the list according to whether they are salt marsh sites or brackish marsh sites and whether they are on the late Lafourche or early Lafourche lobe. Photographs of the classified binary (black and white) maps used to obtain the spatial pattern data are shown for some of the study sites in Figures 11 through 14.

The number of land-water joins (same as interface length) of the 72 sample marsh study sites is shown plotted against their levels of disintegration (percentage open water area) in Figure 15. Lobe and salinity-type are indicated with symbols. Most of the points representing salt marsh sites lie in the upper half of the disintegration scale (50-100%), whereas points for the brackish sites are distributed along the entire scale of disintegration.

The plot demonstrates that maximum interface is reached approximately half way through the disintegration process in real, as well as simulated, marshes, as predicted by Browder et al (1984). The peak in interface in the curve suggested by the plotted points of the sample marshes is slightly offset to the left. Simulations from the improved model with the more powerful G suggest that, under the condition of one water border, high G values in conjunction with low W's cause the peak in interface to shift slightly to the right (Figure 5). Later simulations using W, G, and border-condition values selected for the sample marshes indicate that some W-G-BC conditions cause a shift of interface to the left (Figure 16). Apparently, both G and BC can affect the position of the interface maximum. On the basis of the original model, we predicted that various marshes are on different trajectories of change in interface with disintegration, depending upon the order in which segments of marsh disintegrate and the resultant pattern of land and water. The spread in the curve of plotted points from sample marshes in Figure 15 suggests that this is indeed the case.

The W, G, and border condition selected by the expert system for each sample marsh are shown in Table 3. Note that the selected G values are generally higher for the salt marsh sites than for the brackish marsh sites. This is to be expected since more of the salt marsh sites are on the Gulf of Mexico or on large bays opening onto the Gulf of Mexico. The brackish-marsh sites are more inland, although some are on bodies of water large enough for wind to create considerable turbulence, promoting shoreline erosion. We do not know precisely how large a body of water would have to be for wind-induced turbulence to have a significant effect, but we allowed the expert system to decide when a large water body effect was influencing the spatial pattern of land and water in a given sample marsh study site. The decision was based on the specific spatial pattern statistics of that site. As Table 3 indicates, in most cases, an estimate of W and G with a border condition matching the condition initially defined could be found within the estimates having a high number of water pixels in the estimate. Coefficients of variation ranged from as low as 9% to as high as 807%. Low C.V.s indicate a high degree of convergence of several estimates of W (from the different spatial pattern statistics) from the same G-value and border-condition table; therefore, the lower the C.V., the higher the probable quality of the estimate. The decision number, or number of water pixels used in selection, would have to be divided by the total number of water pixels (192 x 192 x level of disintegration) to use this parameter to estimate the relative quality of the various estimates in Table 3.

Another way of evaluating the quality of the estimated W and G was to reverse our use the look-up tables, determining the spatial pattern sta-

tistics that could be predicted on their basis, given the selected W, G, and border condition for each sample marsh. Table 4 shows results of this analysis, presented in terms of percent agreement on the sides statistics and percent agreement on interface. The interface agreement is the difference between the sample marsh statistic and the predicted statistic, expressed as percentage of sample marsh interface. The agreement on the side-adjacency statistics was determined by summing the absolute value of the difference between sample marsh statistic and predicted statistic for each side-adjacency statistic and expressing this sum as the percent of the total value of the side-adjacency statistics for the sample marsh.

Simulations with the original model indicated that, by affecting the pattern of land and water, the weighting factors of the model affected the way that interface changed with land loss and the maximum interface that was achieved over the complete transition from land to water. We hypothesized that we could select weighting factors to simulate the interface trajectory of a specific disintegrating marsh by comparing its land-water patterns to that of marshes simulated by the model using a range of weighting factor values. Our hypotheses was strengthened and our analyses greatly facilitated by the discovery of an existing theory of spatial autocorrelation (Upton and Fingleton 1985). The "black and white join" statistic of Moran (1948), as described by Upton and Fingleton (1985), is the same as our statistic, interface length, as measured in units of pixel sides. By relating interface of spatial patterns to the weighting factors that simulated those patterns and by showing the dynamics of the change in interface from solid land to solid water, we have contributed to autocorrelation theory.

The fact that W and G had highly-non-linear interactive effects and that the number of water borders affected the force of G and the interaction between G and W greatly complicated our effort to relate spatial patterns to weighting factors. On the other hand, having all three factors to adjust in the model increased our potential for being able to reproduce the spatial patterns of actual marshes, approaching not only their interface but also their side-adjacency statistics. Simulations with the original model, in which W was the only factor having any appreciable effect, could not possibly have been as successful as those we will obtain from the improved model.

We presently are in the process of compiling results from simulations of the disintegration of 70 sample marshes. (Two of the original marshes were in such advanced stages of disintegration that we could not obtain meaningful spatial pattern statistics from them; therefore, we eliminated them from further consideration.) The W-G-BC combinations used to simulate each sample marsh were selected by the expert system on the basis of look-up tables prepared from a series of simulations holding each pair of the factors constant and varying the third in turn. Spatial pattern statistics of the simulated marshes, when at the same level of disintegration as the sample marshes, will be compared to the spatial pattern statistics of the sample marshes to evaluate how successful we have been in matching the spatial pattern parameters and the trajectories of disintegration of the sample marshes.

REFERENCES

Baumann, R. H. Mechanisms of maintaining marsh elevation in a subsiding environment. M. S. Thesis, Louisiana State University, Baton Rouge, 91 p.

Browder, J. A., H. A. Bartley, and K. S. Davis. 1984. A probabilistic model of the relationship between marshland-water interface and marsh disintegration. Ecological Modelling 29:245-260.

Butera, M. K. 1982a. Identification of water bodies using remotely-sensed multispectral scanner data, with applications for inventory, hydrologic assessment, and habitat evaluation. NASA Tech. Memo. No. TM-84672, NASA Earth Resources Laboratory, NSTL, Miss. 18 p.

Butera, M. K. 1982b. A distance measurement derived from Landsat MSS data, with application to marsh productivity, efficient crop transport, and environmental distrubance assessment. NASA TEch. Memo. No. TM-84671, NASA Earth Resources Laboratory, NSTL, Miss. 20 p.

Butera, M. K., and B. R. Seyfarth. 1981. A determination of marsh detrital export from Landsat-MSS data - a function of transport distance and water-body characterization. Proc. Machine Processing of Remotely Sensed Data Symposium. Purdue University, West Lafayette, Indiana.

Butera, M. K., A. L. Frick, and J. A. Browder. 1984. A preliminary report on the assessment of wetland productive capacity from a remote-sensing-based model - a NASA/NMFS joint research project. IEEE Transactions in International Geoscience and Remote Sensing GE-22:502-511.

Cliff, A. D., and J. K. Ord. 1973. Spatial Autocorrelation. Pion: London.

Cowardin, L. M., V. Carter, F. C. Golet, and E. T. LaRoe. 1979. Classification of Wetlands and Deepwater Habitats of the United States. FWS/OBS-79/31, Office of Biological Services, U. S. Fish Wildl. Serv., Washington, D. C. 103 p.

Dow, D. D. 1982. Software programs to measure interface complexity with remote-sensing data, with an example of a marine ecosystem application. NASA Report No. 219. NASA Earth Resources Laboratory, NSTL, Miss. 25 p.

Dow, D. D., and R. W. Pearson. 1982. SLIN: a software program to measure interface length. NASA Earth Resources Laboratory, NSTL, Miss. Report No. 208. 19 pp.

Faller, K. H. 1979. Shoreline as a controlling factor in commercial shrimp production. National Aeronautics and Space Administration, Earth Resources Laboratory, National Space Technology Laboratories, NSTL, MS. NASA Report No. 208. 33 pp.

Gagliano, S. M., K. J. Meyer-Arendt, and K. M. Wicker. 1981. Land loss in the Mississippi River deltaic plain. Transactions Gulf Coast Association of Geological Societies 31:295-300.

Gosselink, J. G. 1984. Th ecology of the delta marshes of coastal Louisiana: a community profile. FWS/OBS-84/09. Office of Biological Services, U. S. Fish Wildl. Serv., 134 p.

Gosselink, J. G., C. C. Cordes, and J. W. Parsons. 1979. An ecological characterization study of the Chenier Plain coastal ecosystem of Louisiana and Texas. FWS/OBS-78/9 through 78/11 (3 vols.). Office of Biological Services, U. S. Fish Wildl. Serv.

Graham, M. H., B. G. Junkin, M. T. Kalcic, R. W. Pearson, and B. R. Seyfarth. 1984. ELAS: Earth Resources Laboratory Applications Software, Vol. 2, ELAS User's Guide. NASA Earth Resources Laboratory, NSTL, Miss. 428 pp.

Hicks, S. D. 1981. Long-period sea-level variations in the United States through 1978. Shore and Beach. Vol. 49. p 26-29.

Hutchinson, G. E. 1957. A Treatise in Limnology. Vol. 1, Part 1. New York: John Wiley. 137 p.

Leibowitz, S. G. and J. M. Hill. In press. Spatial analysis of Louisiana coastal land loss. In R. E. Turner and D. R. Cahoon (eds.). Causes of Wetland Loss in the Coastal Central Gulf of Mexico. Final Report to the Minerals Management Service, New Orleans, LA.

Mandelbrot, B. B. 1967. How long is the coast of Britain? Statistical self similarity and fractional dimension. Science, 56:636-638.

Moran, P. A. P. 1948. The interpretation of statistical maps. Journal of the Royal Statistical society, Series B, 10, 243-251.

Pun, T. 1981. Entropic thresholding, a new approach. Computer Graphics and Image Processing 16:210-239.

Richardson, L. F. 1961. The problem of contiguity: an appendix of statistics of deadly quarrels. Gen. Syst. Yearb. 6:139-187.

Sasser, C. E. 1977. Distribution of vegetation in Louisiana coastal marshes as response to tidal flooding. M. S. Thesis, Louisiana State University, Baton Rouge, 40 p.

Sasser, C.E., M. D. Dozier, J. G. Gosselink, and J. M. Hill. 1986. Spatial and temporal changes in Louisiana's Barataria Basin Marshes, 1945-1980. Environmental Management 10:671-680.

Turner, R. E., K. L. McKee, W. B. Sikora, J. P. Sikora, I. A. Mendelssohn, E. Swenson, C. Neill, S. G. Leibowitz, and F. Pedrazini. 1984. The impact and mitigation of man-made canals in coastal Louisiana. Nat. Sci. Tech. 16:497-504.

Tuttle, J. R., and A. J. Combe. 1981. Flow regime and sediment load affected by alterations of the Mississippi River. p 334-348 in: R. D. Cross and D. L. Williams (eds.). Proc. Natl. Symp. Freshwater Inflow to Estuaries. FWS/OBS-81/04, Office of Biological Services, U. S. Fish Wildl. Serv., Slidell, Louisiana.

Upton, G., and B. Fingleton. 1985. Spatial Data Analysis by Example. Vol. 1. New York: Wiley. 410 p.

Wicker, K. M. 1980. Mississippi deltaic plain region ecological characterization: a habitat mapping study. A User's Guide to the Habitat Maps. FWS/OBS-79/07, Office of Biological Services, U. S. Fish Wildl. Serv., Slidell, Louisiana.

Zimmerman, R. J., T. J. Minello, and G. Zamora, Jr. 1984. Selection of vegetated habitat by brown shrimp, Penaeus aztecus, in a Galveston Bay salt marsh. U. S. Fish. Bull. 82:325-336.

LIST OF TABLES

Table 1. Interface length (synonymous with number of land-water joins) vs. W, G, and border condition, from simulations of 192 x 192-pixel marshes.

		Water Borders					
W	G	1111	1110	1100	1010	1000	0000
0	0	36,695					
4	0	24,946					
20	0	18,243					
60	0	14,357					
180	0	10,921					
540	0	8,113					
0	4		34,573	33,427	33,412	31,888	30,754
4	4		24,801	24,630	24,505	24,243	24,300
20	4		18,516	18,115	18,392	18,264	18,296
60	4		14,434	14,300	14,595	14,385	14,384
180	4		10,726	10,959	10,443	11,053	11,272
540	4		7,672	7,957	8,183	8,156	8,254
0	20		31,208	26,080	28,635	20,395	16,088
4	20		23,401	21,440	22,500	19,311	16,768
20	20		17,924	17,271	17,444	16,867	16,612
60	20		14,273	13,863	14,167	13,766	13,747
180	20		10,937	11,055	10,719	10,999	10,586
540	20		7,940	8,039	7,706	8,058	8,428
0	60		25,752	15,520	20,946	9,667	6,998
4	60		20,540	15,743	18,578	11,001	8,120
20	60		16,791	14,475	16,031	12,348	10,069
60	60		13,777	13,008	13,366	11,792	10,904
180	60		10,771	10,227	10,343	9,927	9,561
540	60		7,789	7,679	7,732	7,895	8,075
0	180		16,113	6,001	9,302	3,836	2,946
4	180		15,994	6,850	10,708	4,251	3,282
20	180		13,866	9,012	11,416	5,402	3,914
60	180		12,481	9,622	11,457	6,687	5,722
180	180		9,919	8,821	9,644	7,551	6,054
540	180		7,789	7,556	7,524	7,404	6,622
0	540		5,961	2,468	3,831	1,939	1,846
4	540		7,093	2,534	4,121	1,979	1,922
20	540		8,826	3,168	5,530	2,205	1,946
60	540		9,322	4,650	7,169	2,737	2,220
180	540		8,513	5,826	7,248	3,693	2,772
540	540		6,877	5,408	6,890	4,572	3,900

1111=no water borders, 1110=one water border, 1100=two adjacent water borders, 1010=two opposite water borders, 1000 = three water borders, 0000=four water borders.

Table 2. Percentage of open water area, number of land-water joins, and number of water pixels by sides adjacent to other water pixels, tabulated from TM images of the salt-marsh study sites.

Quadrangle name	Quarter	Percentage water	Number of land-water joins	Adj-0	Adj-1	Adj-2	Adj-3	Adj-4	Border
Late Lafourche, salt									
Leeville	NW	42.939	9,093	114	439	2,124	2,964	9,856	332
	NE	34.926	10,025	159	713	2,315	2,473	6,860	355
	SE	39.912	10,118	146	519	2,470	2,901	8,369	308
	SW	46.742	6,115	54	253	1,495	2,061	13,064	304
Mink Bayou	NW	26.590	7,166	101	403	1,686	2,067	5,326	219
	NE	24.536	5,519	117	343	1,316	1,289	5,744	236
	SE	29.435	8,420	178	611	1,873	1,977	5,975	237
	SW	29.574	7,937	103	489	1,867	2,192	6,026	225
Caminada Pass	NW	62.093	6,778	80	344	1,669	1,998	18,306	493
	NE	82.867	1,341	3	20	418	411	29,050	646
	SE	99.265	101	0	1	34	25	35,792	741
	SW	58.019	3,884	114	254	952	705	18,845	518
Bay Tambour	NW	51.180	5,818	61	233	1,506	1,788	14,891	388
	NE	76.546	3,047	18	92	773	1,112	25,719	504
	SE	88.723	2,245	24	73	539	826	30,541	704
	SW	84.378	3,515	28	106	833	1,364	28,120	654
Pelican Pass	NW	98.964	341	1	11	67	161	35,491	751
	NE	82.598	2,433	7	93	579	932	28,221	617
	SE	86.683	2,100	13	64	500	839	29,910	629
	SW	97.244	385	0	4	100	160	34,833	751
Early Lafourche,salt									
Grand Bayou du Large	NW	53.833	3,431	48	114	845	1,151	17,371	316
	NE	67.255	3,621	37	158	886	1,145	22,053	514
	SE	40.435	7,174	109	477	1,688	1,839	10,349	444
	SW	83.716	1,111	17	50	254	367	29,643	530

Table 2. (Continued, 2)

Quadrangle name	Quarter	Percentage water	Number of land-water joins	Adj-0	Adj-1	Adj-2	Adj-3	Adj-4	Border
Lake La Graisse	NW	91.132	2,079	17	54	475	853	31,517	679
	NE	99.278	292	0	3	67	143	35,641	744
	SE	100.000	0	0	0	0	0	36,100	764
	SW	99.997	4	0	0	0	4	36,095	764
Central Isles Dernieres	NW	75.770	3,439	31	131	809	1,268	25,018	675
	NE	90.053	1,605	6	33	432	601	31,419	706
	SE	95.182	748	10	18	186	258	33,918	698
	SW	93.533	745	3	12	173	334	33,245	713
Cocodrie	NW	33.434	7,430	106	493	1,692	2,005	7,765	264
	NE	68.894	6,457	40	234	1,454	2,596	20,598	475
	SE	85.786	3,681	32	153	813	1,387	28,656	583
	SW	54.715	9,692	69	410	2,256	3,511	13,522	402
Dog Lake	NW	62.972	4,612	29	159	1,084	1,769	19,788	385
	NE	30.735	8,114	113	449	1,893	2,394	6,218	263
	SE	42.377	7,774	95	403	1,758	2,535	10,514	317
	SW	36.396	6,482	67	331	1,560	1,967	9,106	386
Late Lafourche, brackish									
Lake Bully Camp	NW	33.686	5,689	46	276	1,259	2,079	8,482	276
	NE	47.838	9,158	101	562	2,039	2,845	11,744	344
	SE	22.209	6,157	122	413	1,363	1,578	4,481	230
	SW	50.019	9,502	78	469	2,124	3,373	11,989	406
Golden Meadow Farms	NW	30.914	6,870	81	414	1,530	2,179	6,931	261
	NE	60.693	5,700	80	367	1,181	1,836	18,357	553
	SE	35.558	8,163	86	515	1,813	2,538	7,862	294
	SW	38.949	4,954	47	243	1,085	1,775	11,049	159
Bay L'ours	SE	81.529	3,572	42	254	820	963	27,359	617
	SW	52.257	1,755	34	106	387	513	17,837	387
Three Bayou Bay	SE	32.932	7,393	108	469	1,670	2,108	7,410	375
	SW	58.708	4,136	60	217	974	1,218	18,775	398
Golden Meadow	SW	27.661	9,367	182	709	2,118	2,184	4,802	202

Table 2. (Continued, 3)

Quadrangle name	Quarter	water	Number of land-water joins	Adj-0	Adj-1	Adj-2	Adj-3	Adj-4	Border
Early Lafourche, brackish									
Lost Lake	NW	32.647	6,093	62	329	1,352	2,074	8,031	187
	NE	47.320	9,209	107	550	2,069	2,848	11,576	294
	SE	21.810	7,227	126	496	1,644	1,820	3,689	265
	SW	50.784	8,645	75	442	1,912	3,078	12,874	340
Lake Mechant	NW	64.054	6,070	69	325	1,449	1,836	19,400	534
	NE	29.907	6,782	90	379	1,613	1,957	6,710	267
	SE	44.911	4,570	37	168	1,197	1,471	13,303	380
	SW	67.063	3,050	23	122	823	894	22,310	550
Bayou Sauveur	NW	8.724	3,578	82	291	771	791	1,239	42
	NE	10.902	5,847	160	556	1,201	1,030	966	106
	SE	22.228	5,580	79	323	1,309	1,559	4,721	203
	SW	24.306	4,892	36	199	1,245	1,592	5,748	140
Lake Quitman	NE	48.199	6,983	69	348	1,608	2,326	13,105	312
	SE	32.408	5,981	64	302	1,421	1,881	8,035	244
	SW	31.850	6,545	63	365	1,574	1,948	7,490	301
Dulac	NE	9.633	3,708	82	298	791	883	1,468	29
	SE	66.800	2,710	30	115	666	854	22,739	221
Montegut	SE	47.477	8,315	112	479	1,828	2,657	12,077	349
	SW	27.159	6,787	67	423	1,521	2,103	5,661	237

Adj-0 = number of water pixels with no sides adjacent to water.
Adj-1 = number of water pixels with one sides adjacent to water.
Adj-2 = number of water pixels with two sides adjacent to water.
Adj-3 = number of water pixels with three sides adjacent to water.
Adj-4 = number of water pixels with four sides adjacent to water.
Border = number of water pixels on the border of the sample.

Table 3. W and G weighting factors selected for each study site (sample marsh) by the expert system, with border condition selected (also border condition targeted, if different from one selected), coefficient of variation of the selected W, and number of water pixels involved in the selection.

Quadrant name	Quarter	W	G	Number of water pixels used in selection	C.V. of W (%)	Selected border condition	Targeted border condition
Late Lafourche, salt							
Leeville	NW	272	60	30,887	42	1001	
	NE	188	0	25,395	43	1000	
	SE	237	4	28,599	42	1100	
	SW	8	180	33,905	128	1100	
Mink Bayou	NW	244	180	19,385	46	1010	
	NE	24	180	17,854	115	1100	
	SE	248	0	21,465	58	1000	
	SW	261	180	21,090	45	1110	
Caminada Pass	NW	58	180	43,618	9	1000	
	NE	13	540	60,427	78	1000	1010
	SE	1	540	72,444	225	1100	
	SW	28	540	42,258	32	1100	
Bay Tambour	NW	31	180	35,840	41	1000	
	NE	17	540	55,932	84	1100	
	SE	107	540	64,710	53	1000	
	SW	13	180	61,450	74	1000	
Pelican Pass	NW	8	180	72,202	56	1000	
	NE	88	540	60,281	35	1000	
	SE	16	540	63,217	76	1100	
	SW	38	540	70,941	49	0000	1000
Early Lafourche, salt							
Grand Bayou	NW	30	540	39,374	40	1100	
Du Large	NE	29	540	49,072	36	1100	
	SE	14	180	29,368	95	1100	
	SW	0	540	30,281	211	1100	1110
Lake LaGraisse	NW	113	540	66,511	55	1000	
	NE	10	180	72,382	71	1000	
Central Isles	NW	26	180	55,058	26	0000	
Dernieres	NE	43	540	65,655	70	1000	
	SE	16	540	69,460	26	1000	1010
	SW	33	540	68,235	43	0000	1000
Cocodrie	NW	115	180	23,893	72	1010	
	NE	311	540	50,085	55	1110	
	SE	69	540	61,852	15	1100	
	SW	233	60	39,528	30	1100	
Dog Lake	NW	44	540	46,043	65	1100	1110
	NE	213	180	21,948	32	1010	
	SE	120	180	30,927	56	1100	
	SW	123	540	26,448	61	1110	1010

Table 3. (continued).

Quadrant name	Quarter	W	G	Number of water pixels used in selection	C.V. of W (%)	Selected border condition	Targeted border condition
Late Lafourche, brackish							
Lake Bully Camp	NW	62	180	24,560	90	1000	
	NE	244	180	34,926	52	1110	
	SE	130	60	15,731	88	1100	
	SW	255	60	36,472	41	0000	
Golden Meadow Farm	NW	129	180	22,531	45	1100	
	NE	160	540	44,195	14	1100	
	SE	308	60	25,407	47	1100	
	SW	3,184	0	28,557	53	1111	1110
Bay L'ours	SE	8	180	59,493	58	1000	
	SW	1	540	18,877	807	1100	
Three Bayou Bay	SE	100	60	23,905	80	0000	
	SW	33	540	42,886	43	1100	1110
Golden Meadow	SW	116	0	20,192	82	1100	
Early Lafourche, brackish							
Lost Lake	NW	23	180	23,883	131	1100	
	NE	245	180	34,594	53	1110	
	SE	111	60	15,815	66	1000	
	SW	290	20	36,660	61	1000	
Lake Mechant	NW	4	180	46,367	132	1100	
	NE	118	60	21,404	86	1100	
	SE	86	540	31,535	35	1100	
	SW	17	540	48,894	81	1100	
Bay Sauveur	NW	325	0	6,390	78	1111	
	NE	93	0	7,932	61	1111	
	SE	133	180	16,185	45	1100	
	SW	35	540	17,780	141	1110	
Lake Quitman	NE	116	540	34,876	75	1110	
	SE	20	180	23,650	110	1100	
	SW	121	180	23,181	52	1100	1000
Dulac	NE	701	0	7,073	39	1111	
	SE	10,947	0	———	—	1111	
Montegut	SE	289	180	34,176	59	1010	
	SW	404	0	19,787	70	1111	

Table 4. Look-up table based predictions of success of model with expert-system-selected W and G in simulating marshes with spatial patterns fitting those of study sites (sample marshes).

Quadrangle name	Quadrant	Disinteg. level	W	G	% Agree sides	% Agree interface
Late Lafourche, salt						
Leeville	NW	0.4294	272	60	94.69	96.37
	NE	0.3493	188	0	92.47	99.81
	SE	0.3991	237	4	94.03	99.57
	SW	0.4674	8	180	88.63	84.16
Mink Bayou	NW	0.2659	244	180	94.13	98.38
	NE	0.2454	24	180	88.66	90.58
	SE	0.2944	248	0	90.47	93.86
	SW	0.2957	261	180	94.55	99.30
Caminada Pass	NW	0.6209	58	180	98.32	97.33
	NE	0.8287	13	540	98.92	95.92
	SE	0.9926	1	540	99.90	94.06
	SW	0.5802	28	540	97.40	96.14
Bay Tambour	NW	0.5118	31	180	93.35	99.35
	NE	0.7655	17	540	96.73	99.27
	SE	0.8872	107	540	99.13	89.98
	SW	0.8438	13	180	97.28	97.21
Pelican Pass	NW	0.9896	8	180	99.78	98.53
	NE	0.8260	88	540	98.76	95.81
	SE	0.8668	16	540	98.20	98.55
	SW	0.9724	38	540	99.76	93.25
Early Lafourche, salt						
Grand Bayou du Large	NW	0.5383	30	540	95.41	92.73
	NE	0.6726	29	540	96.87	97.34
	SE	0.4044	14	180	90.35	93.79
	SW	0.8372	0	540	98.84	67.54
Lake LaGraisse	NW	0.9113	113	540	99.07	87.64
	NE	0.9928	10	180	99.75	84.25
Central Isles Dernieres	NW	0.7577	26	180	97.74	94.63
	NE	0.9005	43	540	98.99	90.84
	SE	0.9518	16	540	99.76	96.52
	SW	0.9353	33	540	99.49	95.44
Cocodrie	NW	0.3343	115	180	88.96	80.65
	NE	0.6889	311	540	97.41	88.84
	SE	0.8579	69	540	99.32	98.72
	SW	0.5471	233	60	96.55	99.38
Dog Lake	NW	0.6297	44	540	95.16	96.27
	NE	0.3073	213	180	95.30	99.03
	SE	0.4238	120	180	95.29	87.52
	SW	0.3640	123	540	93.75	79.62

Table 4. Continued.

Quadrangle name	Quadrant	Disinteg. level	W	G	% Agree sides	% Agree interface
Late Lafourche, brackish						
Lake Bully Camp	NW	0.3369	62	180	92.50	96.10
	NE	0.4784	244	180	95.73	96.50
	SE	0.2221	130	60	79.42	71.35
	SW	0.5002	255	60	96.44	97.36
Golden Meadow Farms	NW	0.3091	129	180	95.25	89.58
	NE	0.6069	160	540	99.00	95.94
	SE	0.3556	308	60	93.91	93.42
	SW	0.3895	3,184	0	97.46	93.99
Bay L'ours	SE	0.8153	8	180	97.61	93.31
	SW	0.5226	1	540	97.53	70.57
Three Bayou Bay	SE	0.3293	100	60	84.92	75.97
	SW	0.5871	33	540	95.78	95.65
Golden Meadow	SW	0.2766	116	0	87.87	86.64
Early Lafourche, brackish						
Lost Lake	NW	0.3265	23	180	89.61	83.40
	NE	0.4732	245	180	95.51	97.22
	SE	0.2181	111	60	88.73	88.17
Lake Mechant	NW	0.6405	4	180	92.66	85.34
	NE	0.2991	118	60	80.35	66.44
	SE	0.4491	86	540	95.74	97.30
	SW	0.6706	17	540	96.41	96.46
Bay Sauveur	NW	0.0872	325	0	88.54	86.70
	NE	0.1090	93	0	90.33	89.32
	SE	0.2223	133	180	92.79	87.31
	SW	0.2431	35	540	88.09	80.33
Lake Quitman	NE	0.4820	116	540	93.82	78.86
	SE	0.3241	20	180	89.58	82.80
	SW	0.3185	121	180	94.27	84.09
Dulac	NE	0.0963	701	0	95.94	96.22
	SE	0.			N.A.	N.A.
Montegut	SE	0.4748	289	180	94.85	93.09
	SW	0.2716	404	0	93.74	88.63

LIST OF APPENDIX TABLES

LIST OF FIGURES

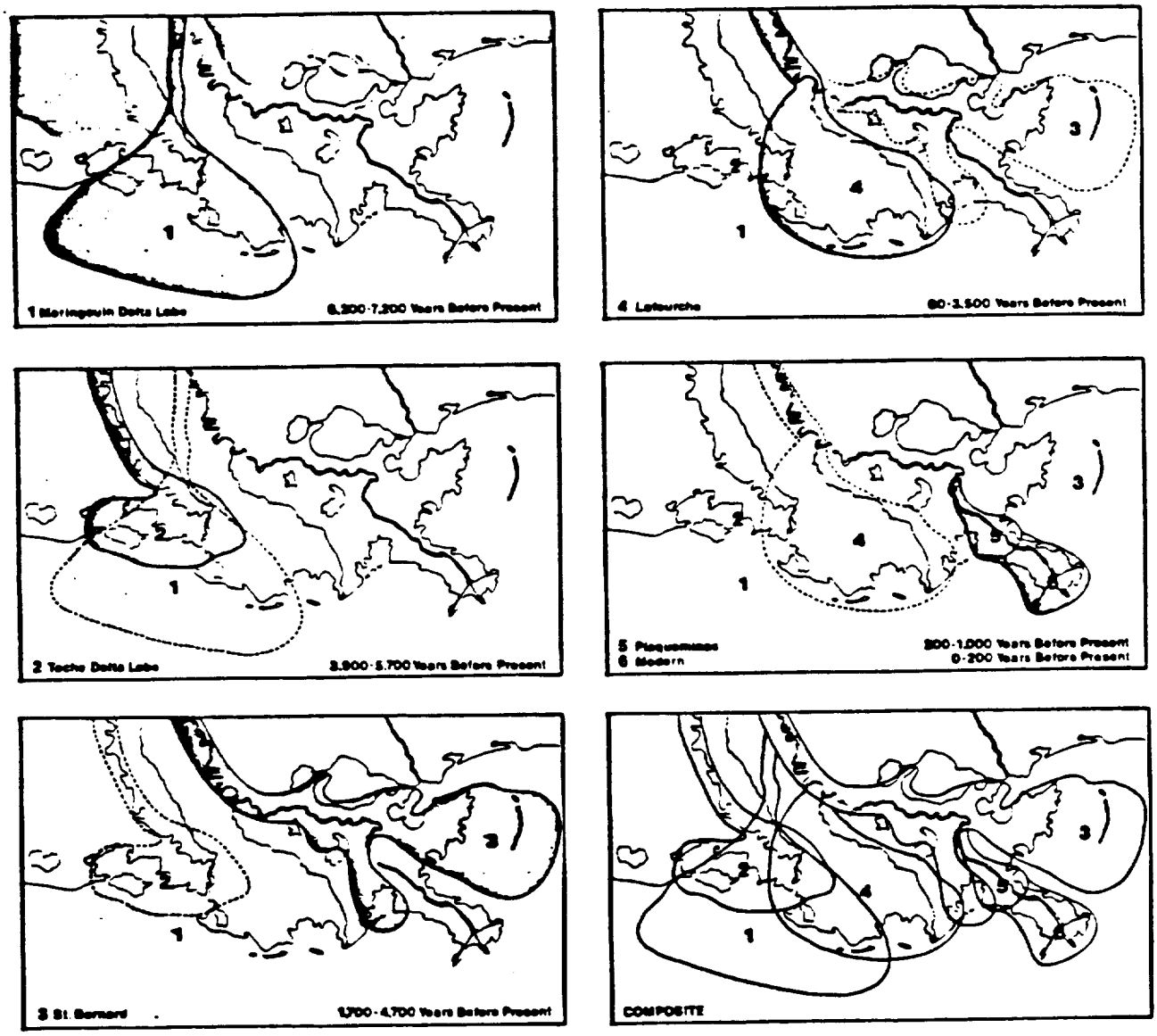

Figure 1. The maximum extent of deltaic lobes of the Mississippi River influencing the present geomorphology of Louisiana's coastal wetlands.

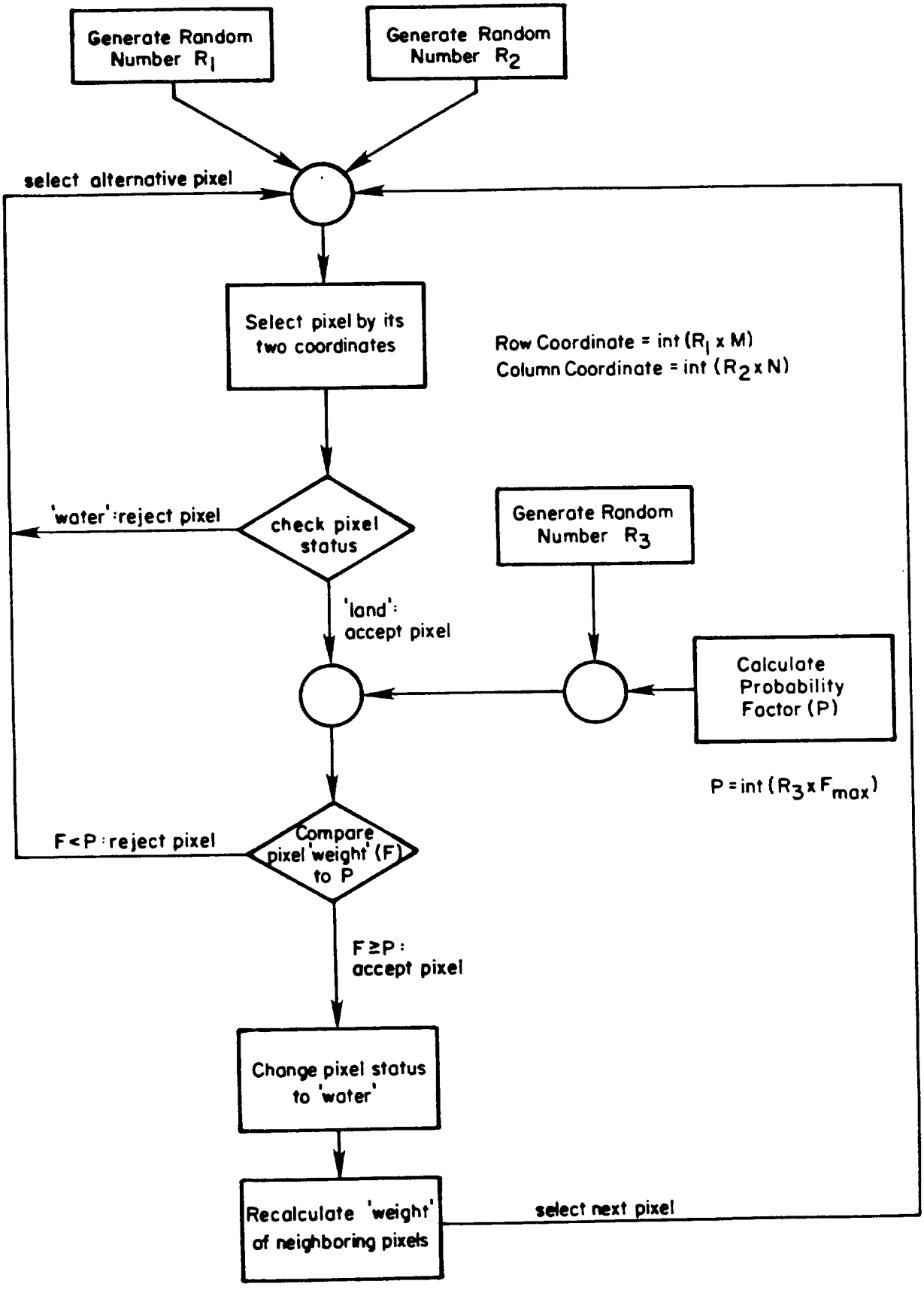

R_1, R_2, and R_3 = random numbers between 0 and 1, reselected at each iteration

F = 'weight' of selected pixel

F_{max} = maximum 'weight' on land list

Figure 2. Flow diagram of algorithm for selection of pixel to be disintegrated at each iteration of the model.

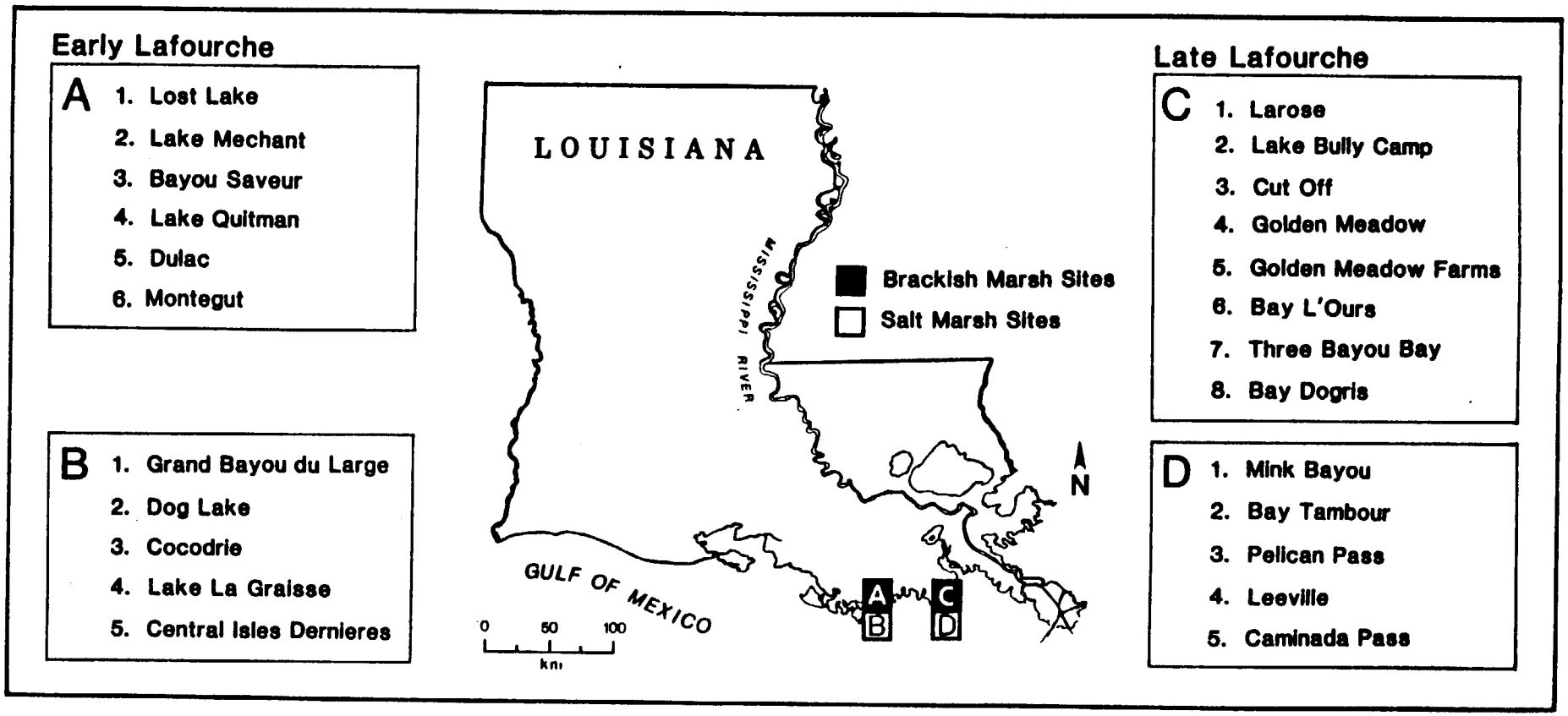

Figure 3. Location of salt and brackish marsh study sites on the early and late Lafourche lobes. Listed names refer to specific U.S. Geological 7.5-minute topographic maps used in the study; they are listed by marsh type and deltaic lobe.

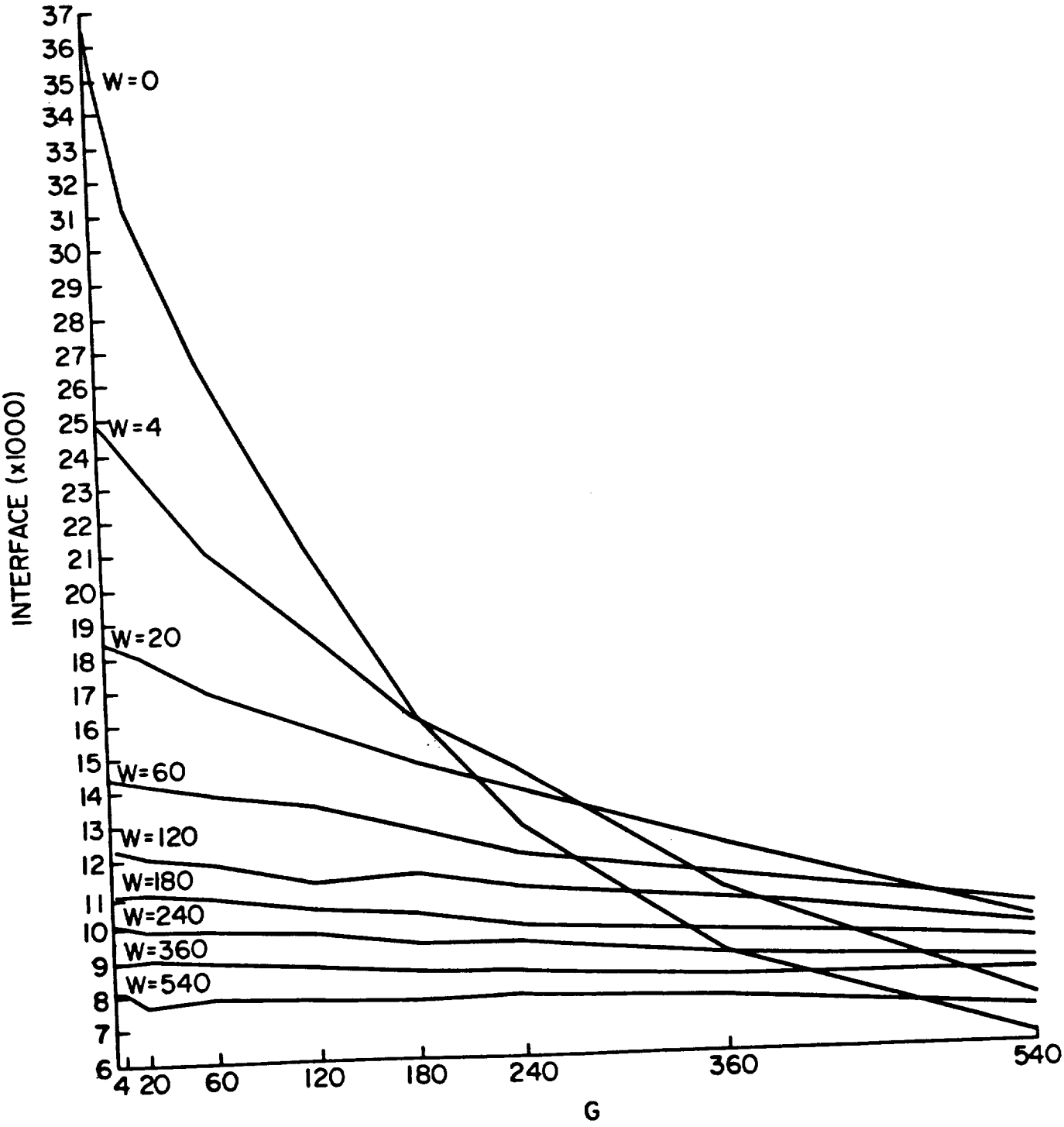

Figure 4. Variation in interface with W and G in simulated 48 x 48-pixel marshes with one water border.

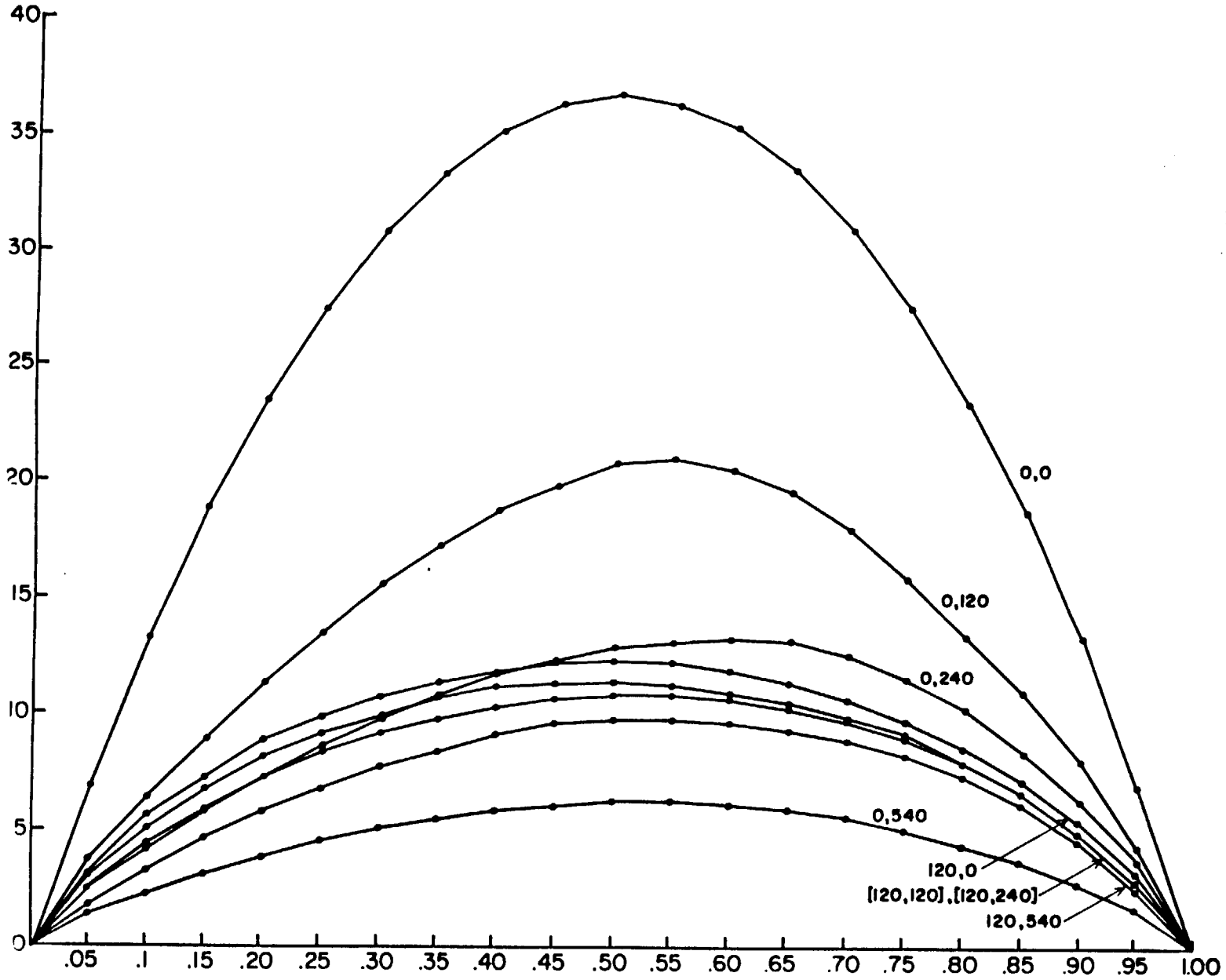

Figure 5. Change in interface with disintegration for different values of W (first in pair of values) and G in simulations of 48 x 48-pixel marshes with one water border.

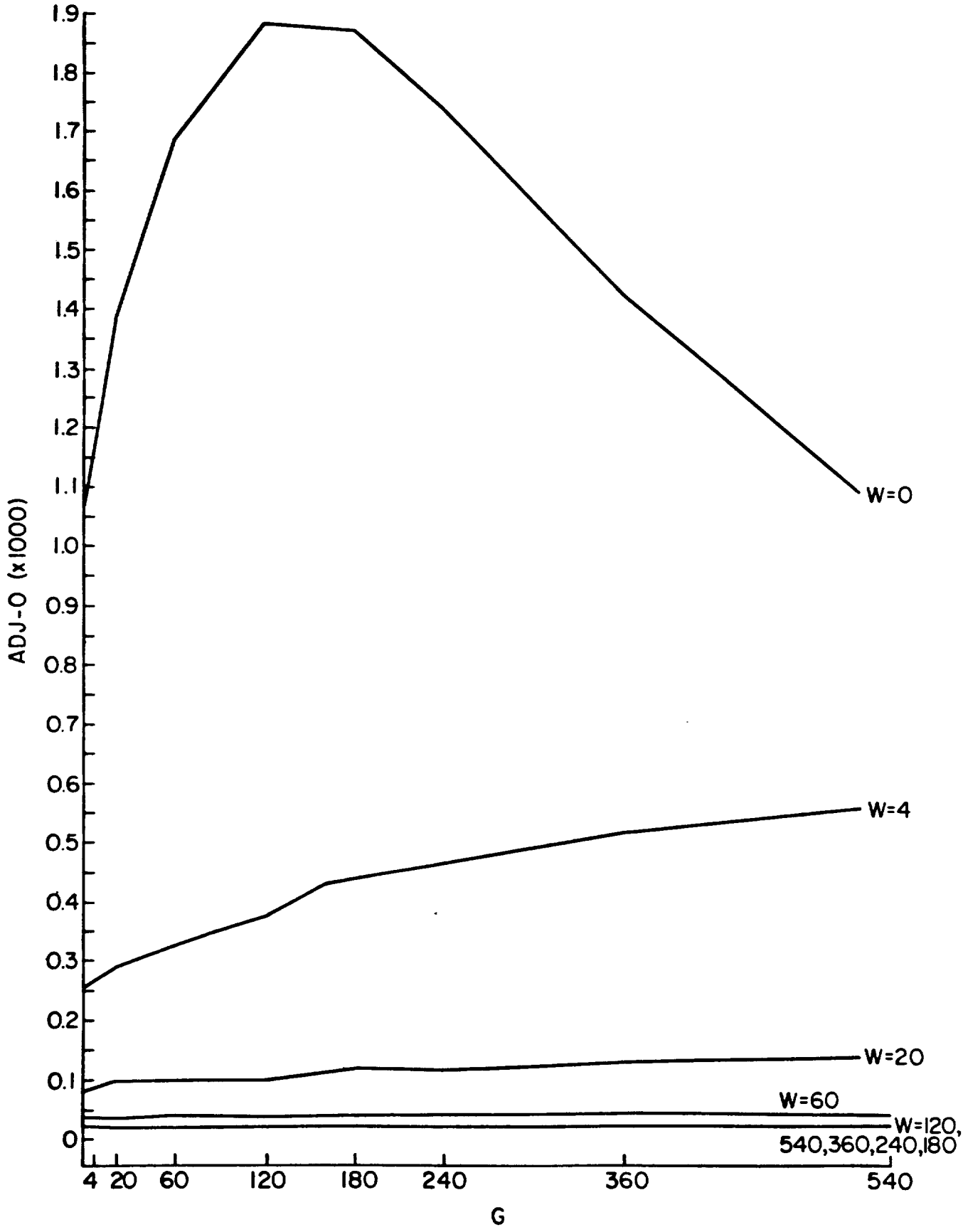

Figure 6. Variation in the side-adjacency-0 statistic with W and G in simulated 48 x 48-pixel marshes with one water border.

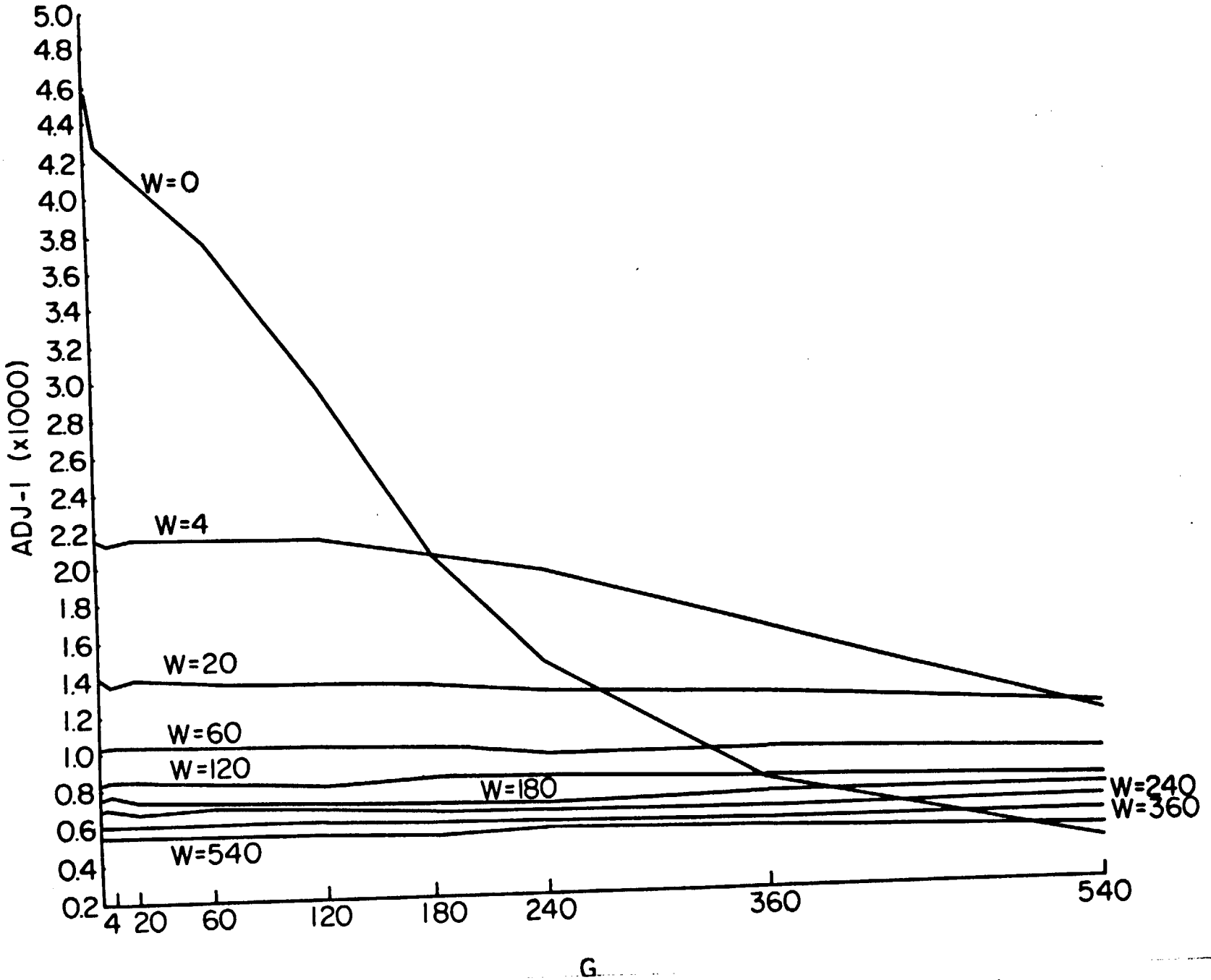

Figure 7. Variation in the side-adjacency-1 statistic with W and G in simulated 48 x 48-pixel marshes with one water border.

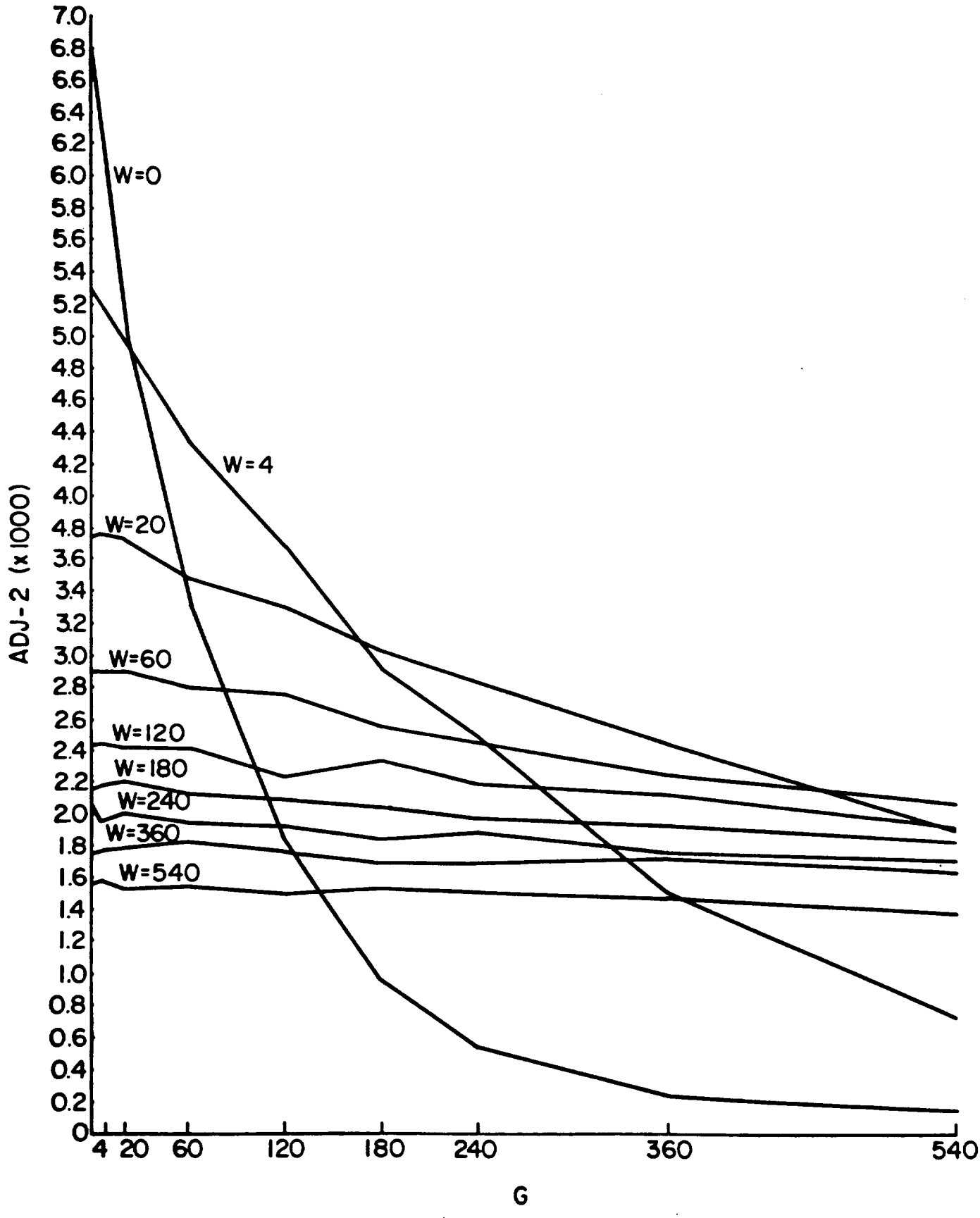

Figure 8. Variation in the side-adjacency-2 statistic with W and G in simulated 48 x 48-pixel marshes with one water border.

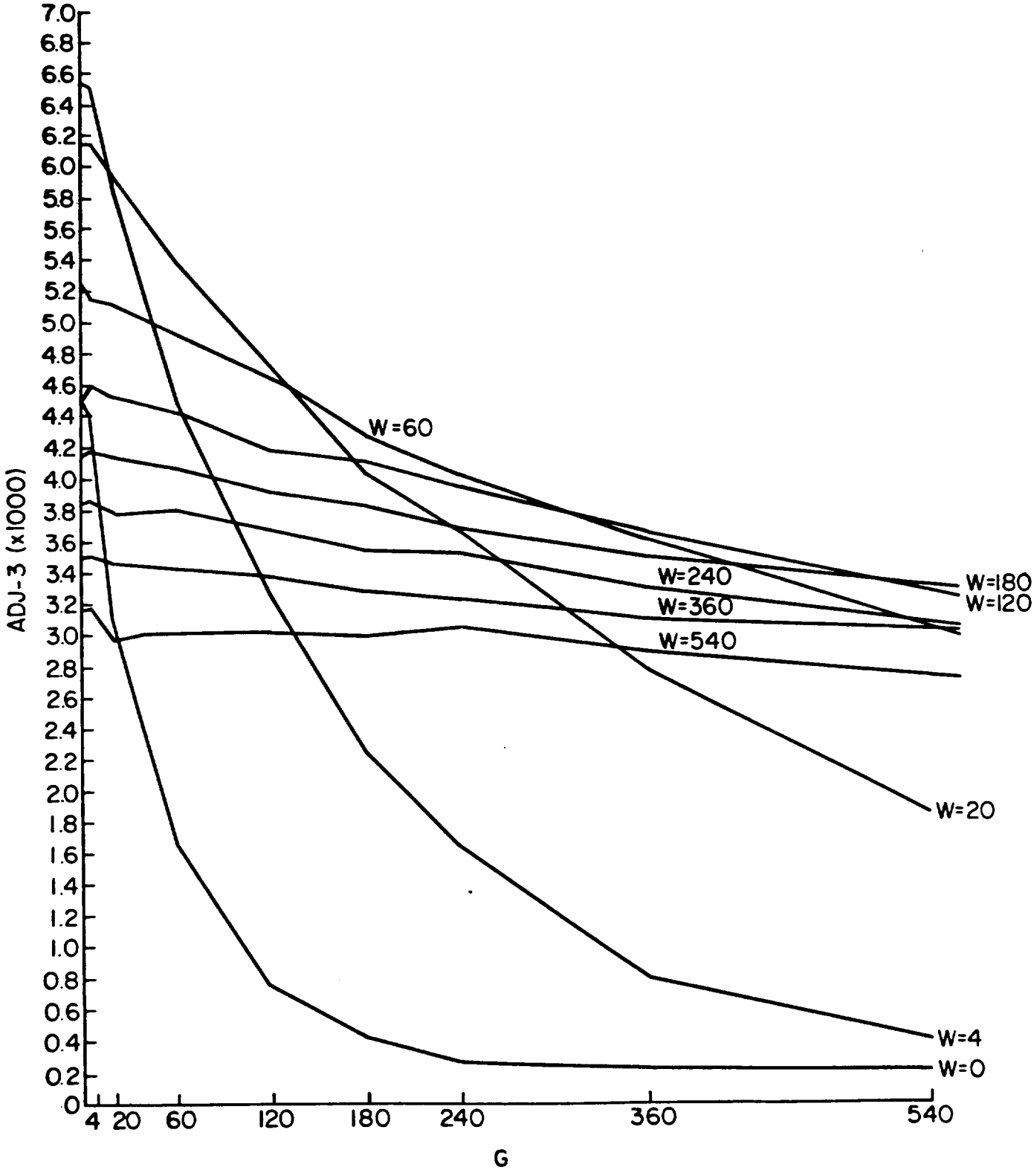

Figure 9. Variation in the side-adjacency-3 statistic with W and G in simulated 48 x 48-pixel marshes with one water border.

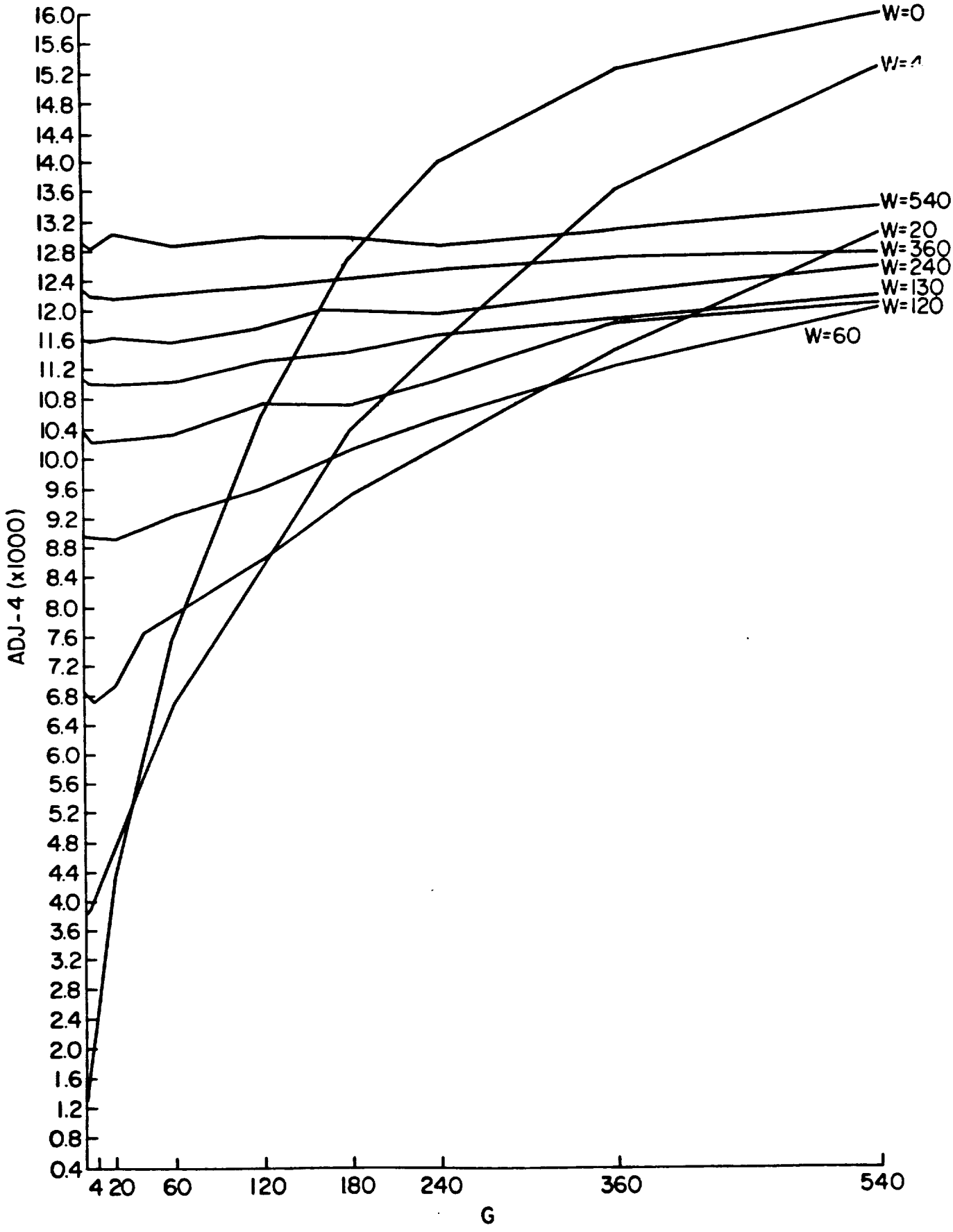

Figure 10. Variation in the side-adjacency-4 statistic with W and G in simulated 48 x 48-pixel marshes with one water border.

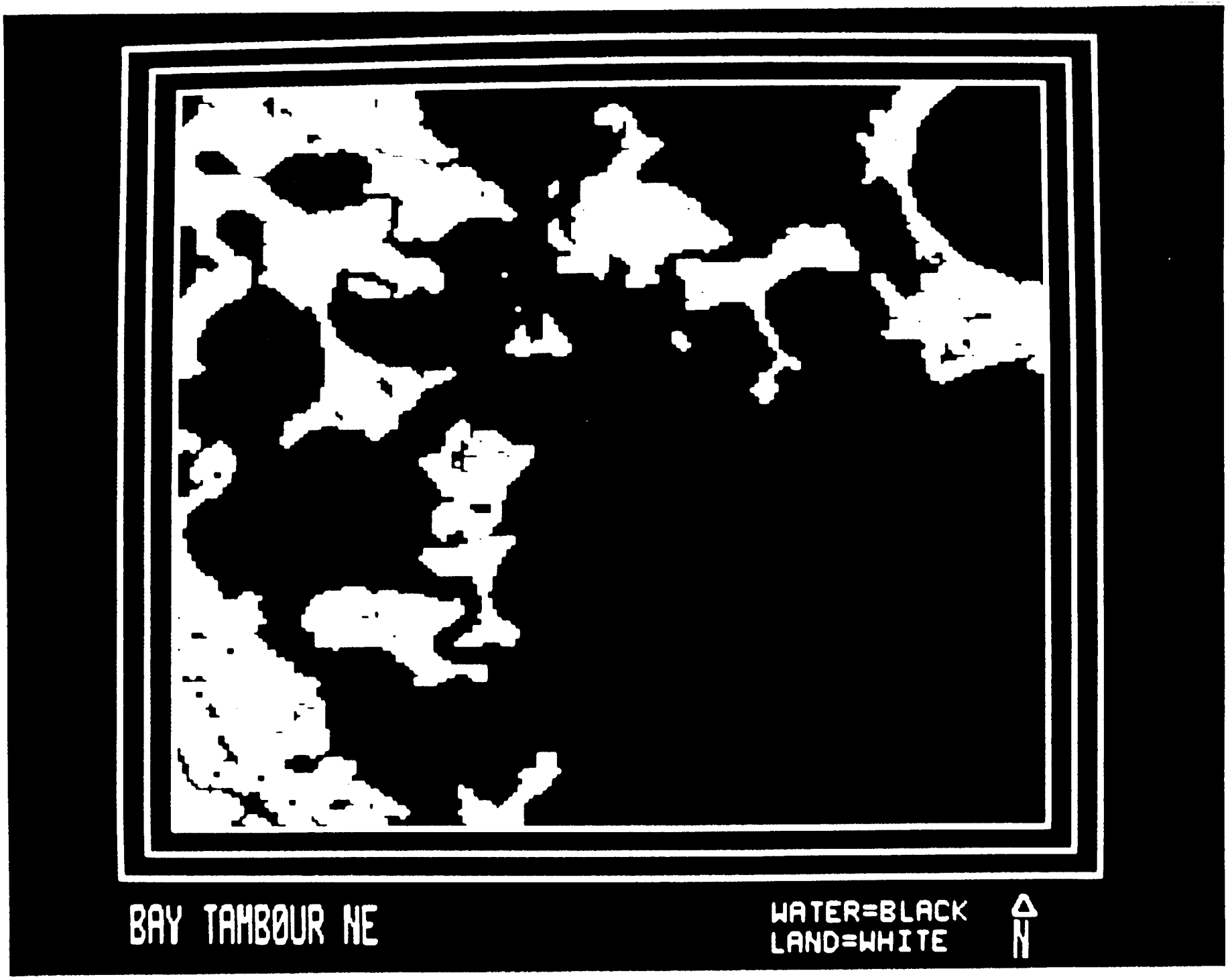

Figure 11. Photograph of classified binary (land=white, water=black) map of sample marsh study site; example of late Lafourche salt marsh site.

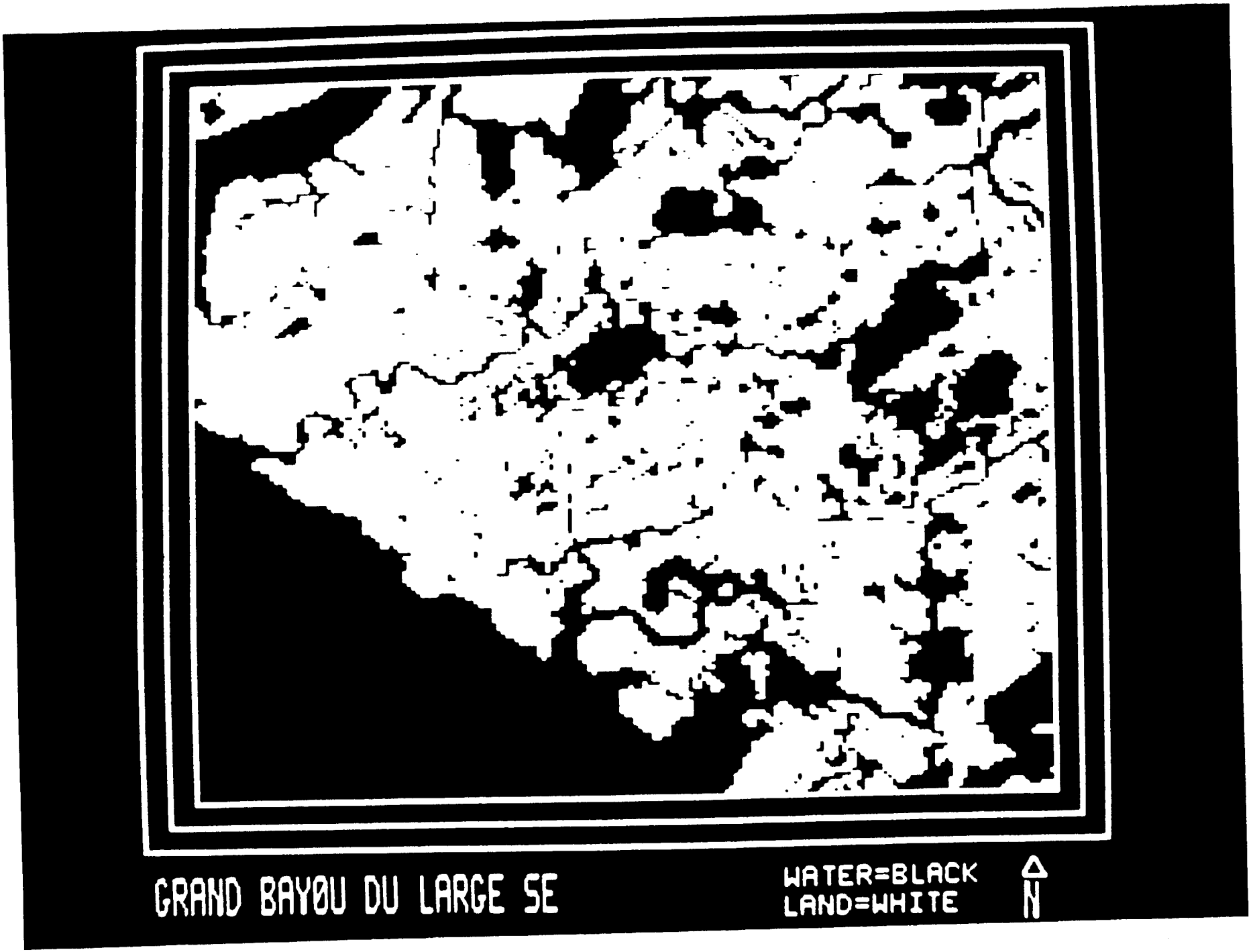

Figure 12. Photograph of classified binary (land=white, water=black) map of sample marsh study site; example of early Lafourche salt marsh site.

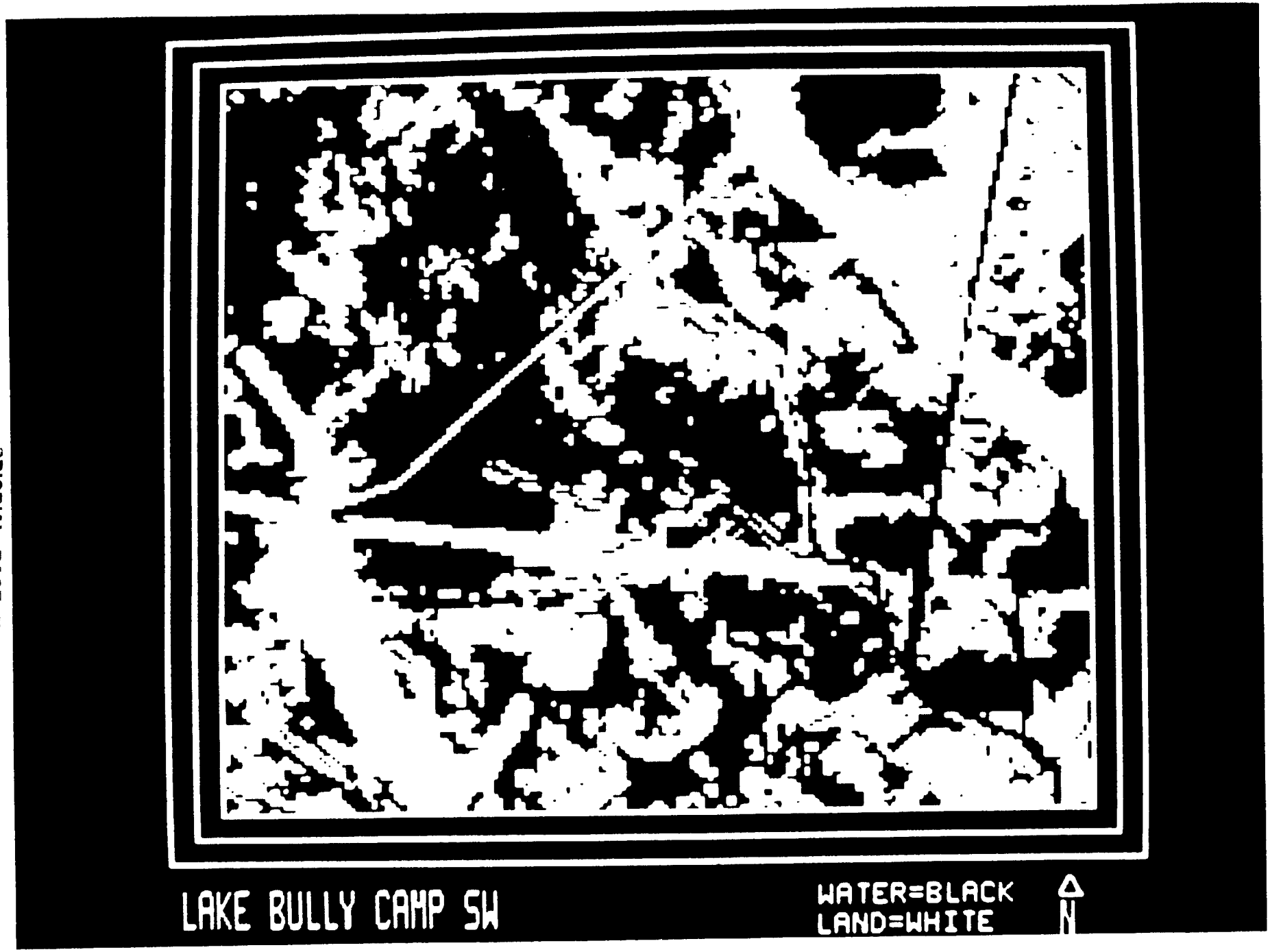

Figure 13. Photograph of classified binary (land=white, water=black) map of sample marsh study site; example of late Lafourche brackish marsh site.

Figure 14. Photograph of classified binary (land=white, water=black) map of sample marsh study site; example of early Lafourche brackish marsh site.

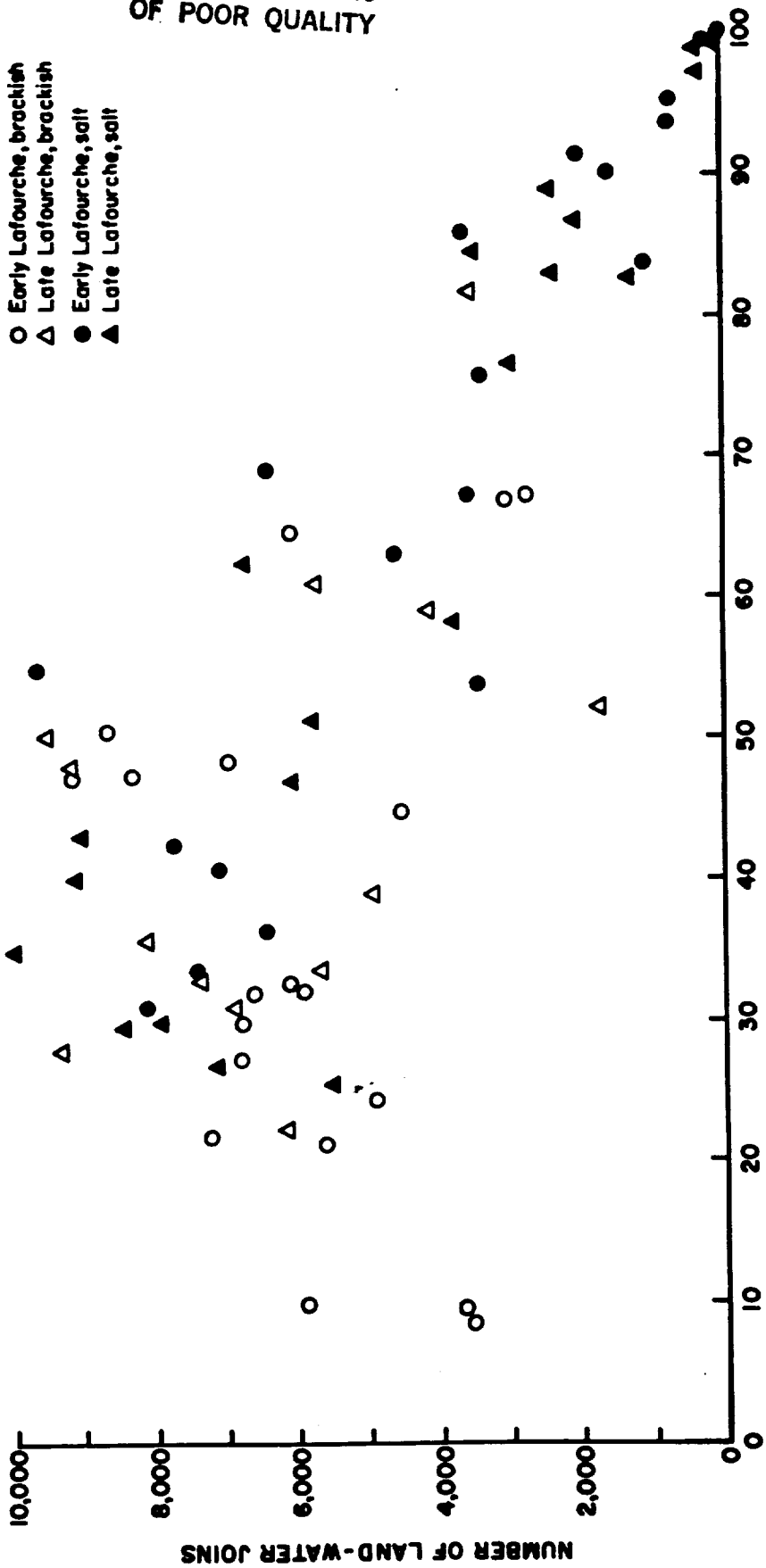

Figure 15. Plot of measured land-water joins (same as interface length) vs level of disintegration of sample marsh study sites.

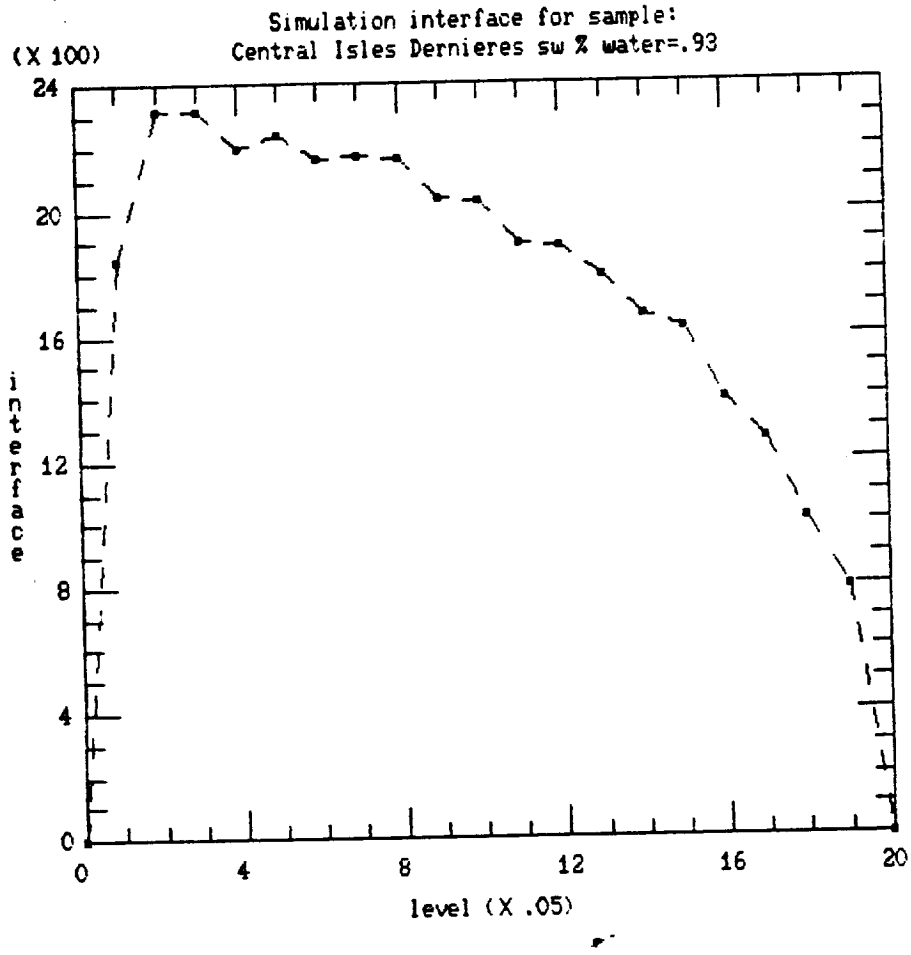

W = 33
G = 540

Four water borders

Figure 16. Plot of interface with disintegration of a sample marsh study site.

Appendix Table 1. Look-up table used to classify water and land identified by the ELAS shoreline length (SLIN) module into water pixels and land pixels with zero, one, two, three, and four sides adjacent to water.

SLIN output	Class code	SLIN output	Class code	SLIN output	Class code
0	5	24	2	48	3
1	0	25	1	49	3
2	0	26	1	50	2
3	1	27	2	51	2
4	0	28	2	52	2
5	0	29	2	53	3
6	1	30	2	54	3
7	1	31	2	55	3
8	0	32	2	56	3
9	1	33	2	57	3
10	1	34	2	58	3
11	0	35	1	59	3
12	2	36	2	60	3
13	1	37	2	61	3
14	1	38	2	62	3
15	1	39	2	63	3
16	1	40	2	64	3
17	1	41	2	65	4
18	1	42	2	66	4
19	2	43	2	67	4
20	2	44	2	68	4
21	1	45	2	69	4
22	1	46	3	70	ND
23	2	47	3	71	ND

Key to Class Codes:
0 = land pixel with zero sides adjacent to water.
1 = land pixel with one side adjacent to water.
2 = land pixel with two sides adjacent to water.
3 = land pixel with three sides adjacent to water.
4 = land pixel with four sides adjacent to water.
5 = water pixel.

Appendix Table 2. Interface length at 0.5 disintegration level, from simulations of 192 x 192-pixel marshes, listed in order from largest to smallest, with W, G, and border condition indicated.

W	G	Border Condition	Interface Length
0	0	1111	36,695
0	4	1110	34,573
0	4	1100	33,427
0	4	1010	33,412
0	4	1000	31,888
0	20	1110	31,208
0	4	0000	30,754
0	20	1010	28,635
0	20	1100	26,080
0	60	1110	25,752
0	0	1111	24,946
4	4	1110	24,801
4	4	1100	24,630
4	4	1010	24,505
4	4	0000	24,300
4	4	1000	24,243
4	20	1110	23,401
4	20	1010	22,500
4	20	1100	21,440
0	60	1010	20,946
4	60	1110	20,540
0	20	1000	20,395
4	20	1000	19,311
4	60	1010	18,578
20	4	1110	18,516
20	4	1010	18,392
20	4	0000	18,296
20	4	1000	18,264
20	0	1111	18,243
20	4	1100	18,115
20	20	1110	17,924
20	20	1010	17,444
20	20	1100	17,271

Appendix Table 2. (continued 2).

W	G	Border Condition	Interface Length
20	20	1000	16,867
20	60	1110	16,791
4	20	0000	16,768
20	20	0000	16,612
0	180	1110	16,113
0	20	0000	16,088
20	60	1010	16,031
4	180	1110	15,994
4	60	1100	15,743
0	60	1100	15,520
60	4	1010	14,595
20	60	1100	14,475
60	4	1110	14,434
60	4	1000	14,385
60	4	0000	14,384
60	4	1100	14,300
60	0	1111	14,357
60	20	1110	14,273
60	20	1010	14,167
20	180	1110	13,866
60	20	1100	13,863
60	20	1000	13,766
60	60	1110	13,777
60	20	0000	13,747
60	60	1010	13,366
60	60	1100	13,008
60	180	1110	12,481
20	60	1000	12,348
60	60	1000	11,792
60	180	1010	11,457
20	180	1010	11,416
180	4	0000	11,272
180	20	1100	11,055
180	4	1000	11,053
4	60	1000	11,001
180	20	1000	10,999
180	4	1100	10,959
180	20	1110	10,937
180	0	1111	10,921
60	60	0000	10,904

Appendix Table 2. (continued 3).

W	G	Border Condition	Interface Length
180	60	1110	10,771
180	4	1110	10,726
180	20	1010	10,719
4	180	1010	10,708
180	20	0000	10,586
180	4	1010	10,443
180	60	1010	10,343
180	60	1100	10,227
20	60	0000	10,069
180	60	1000	9,927
180	180	1110	9,919
0	60	1000	9,667
180	180	1010	9,644
60	180	1100	9,622
180	60	0000	9,561
60	540	1110	9,322
0	180	1010	9,302
20	180	1100	9,012
20	540	1110	8,826
180	180	1100	8,821
180	540	1110	8,513
540	20	0000	8,428
540	4	0000	8,254
540	4	1010	8,183
540	4	1000	8,156
4	60	0000	8,120
540	0	1111	8,113
540	60	0000	8,075
540	20	1000	8,058
540	20	1100	8,039
540	4	1100	7,957
540	20	1110	7,940
540	60	1000	7,895
540	60	1110	7,789
540	180	1110	7,789
540	60	1010	7,732
540	20	1010	7,706
540	60	1100	7,679
540	4	1110	7,672
540	180	1100	7,556
180	180	1000	7,551
540	180	1010	7,524
540	180	1000	7,404
180	540	1010	7,248
60	540	1010	7,169
4	540	1110	7,093

Appendix Table 2. (continued 4).

W	G	Border Condition	Interface Length
0	60	0000	6,998
540	540	1010	6,890
540	540	1110	6,877
4	180	1100	6,850
60	180	1000	6,687
540	180	0000	6,622
180	180	0000	6,054
0	180	1100	6,001
0	540	1110	5,961
180	540	1100	5,826
60	180	0000	5,722
20	540	1010	5,530
540	540	1100	5,408
20	180	1000	5,402
60	540	1100	4,650
540	540	1000	4,572
4	180	1000	4,251
4	540	1010	4,121
20	180	0000	3,914
540	540	0000	3,900
0	180	1000	3,836
0	540	1010	3,831
180	540	1000	3,693
4	180	0000	3,282
20	540	1100	3,168
0	180	0000	2,946
180	540	0000	2,772
60	540	1000	2,737
4	540	1100	2,534
0	540	1100	2,468
60	540	0000	2,220
20	540	1000	2,205
4	540	1000	1,979
20	540	0000	1,946
0	540	1000	1,939
4	540	0000	1,922
0	540	0000	1,846